B. Siemon, A. Ullmann, M. Ibs-von Seht,
W. Voß, J. Pielawa

BGR Bundesanstalt für Geowissenschaften und Rohstoffe

Airborne Geophysical Investigations of CLIWAT Pilot Areas

Survey Area Friesland, The Netherlands, 2009

CLIWAT
CLIMATE & WATER

The Interreg IVB North Sea Region Programme
Investing in the future by working together for a sustainable and competitive region

Interreg IVB Project:
CLIWAT – Adaptive and sustainable water management and protection of society and nature in an extreme climate

Bundesanstalt für Geowissenschaften und Rohstoffe
Federal Institute for Geosciences and Natural Resources

CLIWAT – Adaptive and sustainable water management and protection of society and nature in an extreme climate

Survey Area Friesland, The Netherlands

2009

Technical Report on the Interreg IVB Project

The project is part-financed by the European Union

In Cooperation with
TNO
Deltares
Wetterskip Fryslân
Provincje Fryslân

Authors: B. Siemon
A. Ullmann
M. Ibs-von Seht
W. Voß
J. Pielawa

Date: December 15, 2010

Table of contents

Personnel

Field Crew

Dr. Bernhard **Siemon**, project leader, field data processing, B2.1, BGR
Angelika **Ullmann**, project scientist, field data processing, B2.1, BGR
Wolfgang **Voß**, navigation, B2.1, BGR
Karl-Heinz **Meinhardt**, system operation and engineering, B2.1, BGR
Josef **Scheiwein**, helicopter engineering, B2.1, BGR
Michael **Schütt**, pilot, Wiking Helikopter Service GmbH

Office Crew

Dr. Uwe **Meyer**, leader of sub-department B2.1, BGR
Dr. Bernhard **Siemon**, project leader, electromagnetic data evaluation, B2.1, BGR
Angelika **Ullmann**, project scientist, electromagnetic data evaluation, B2.1, BGR
Dr. Malte **Ibs-von Seht**, magnetic and radiometric data evaluation, B2.1, BGR
Jens **Pielawa**, cartographic work, B2.1, BGR

Address:

Federal Institute for Geosciences and Natural Resources (BGR)
Stilleweg 2
30655 Hanover
Germany
Tel.: +49 511 643 3212 (Meyer)
3488 (Siemon)
Fax: +49 511 643 3663
Email: Uwe.Meyer@bgr.de, Bernhard.Siemon@bgr.de

List of figures:

List of tables:

List of maps:

1. Flight lines,
2. Digital elevation model,
3. Apparent resistivity at 133,300 Hz (rhoa6),
4. Apparent resistivity at 41,460 Hz (rhoa5),
5. Apparent resistivity at 8,388 Hz (rhoa4),
6. Apparent resistivity at 5,405 Hz (rhoa3),
7. Apparent resistivity at 1,821 Hz (rhoa2),
8. Apparent resistivity at 387 Hz (rhoa1),
9. Centroid depth at 133,300 Hz (zst6),
10. Centroid depth at 41,460 Hz (zst5),
11. Centroid depth at 8,388 Hz (zst4),
12. Centroid depth at 5,405 Hz (zst3),
13. Centroid depth at 1,821 Hz (zst2),
14. Centroid depth at 387 Hz (zst1),
15. Resistivity at 02 m bgl,
16. Resistivity at 04 m bgl,
17. Resistivity at 06 m bgl,
18. Resistivity at 08 m bgl,
19. Resistivity at 10 m bgl,
20. Resistivity at 15 m bgl,
21. Resistivity at 20 m bgl,
22. Resistivity at 25 m bgl,
23. Anomalies of the total magnetic field (ΔT),
24. Concentration of Potassium (K),
25. Concentration of Thorium (Th),
26. Concentration of Uranium (U),
27. Stripped total count rate (TC),
28. Ground level exposure rate in µR/h.

All maps were produced for two 1:25.000 map sheets: SW and NE.

List of vertical resistivity sections:

Tie lines:

1. VRS 1.9,
2. VRS 2.9,
3. VRS 3.9,
4. VRS 4.9,
5. VRS 5.9,
6. VRS 10.9,
7. VRS 11.9,
8. VRS 12.9.

Lines:

9. VRS 2.1,
10. VRS 3.1,
11. VRS 4.1,
12. VRS 5.1,
13. VRS 6.1,
14. VRS 7.1,
15. VRS 8.3,
16. VRS 9.3,
17. VRS 10.1,
18. VRS 10.3,
19. VRS 11.1,
20. VRS 11.3,
21. VRS 12.1,
22. VRS 12.3,
23. VRS 13.1,
24. VRS 13.3,
25. VRS 14.1,
26. VRS 14.3,
27. VRS 15.1,
28. VRS 15.3,
29. VRS 16.1,
30. VRS 16.3,
31. VRS 17.1,
32. VRS 17.3,
33. VRS 18.1,
34. VRS 18.3,
35. VRS 19.1,
36. VRS 19.3,
37. VRS 20.1,
38. VRS 20.3,
39. VRS 21.1,
40. VRS 21.3,
41. VRS 22.1,
42. VRS 22.3,
43. VRS 23.1,
44. VRS 23.3,
45. VRS 24.1,
46. VRS 24.3,
47. VRS 25.1,
48. VRS 25.3,
49. VRS 26.1,
50. VRS 26.3,
51. VRS 27.1,
52. VRS 27.4,
53. VRS 28.1,
54. VRS 28.3,
55. VRS 29.1,
56. VRS 29.3,
57. VRS 30.1,
58. VRS 30.3,
59. VRS 31.1,
60. VRS 31.3,
61. VRS 32.1,
62. VRS 32.3,
63. VRS 33.1,
64. VRS 33.4,
65. VRS 34.1,
66. VRS 34.3,
67. VRS 35.1,
68. VRS 35.3,
69. VRS 36.1,
70. VRS 37.1,
71. VRS 38.1,
72. VRS 39.1,
73. VRS 40.1,
74. VRS 41.1,
75. VRS 42.1.

Abbreviations

°	degree
°C	degree Celsius
'	minute
"	second or inch
%	per cent
1-D	one-dimensional
a	aircraft background
A	amplitude of measured HEM components
A_c, A'_c	amplitudes of calculated HEM components
A'_p	polynomial approximation of $A'_c(\delta)$
Ah	ampere hours
agl	above ground level
asl	above mean sea level
α, β, γ, a	stripping ratios
α_e, β_e , γ_e	height corrected stripping ratios
α_0	complex wave number
b	cosmic stripping factor
bgl	below ground level
BGR	Bundesanstalt für Geowissenschaften und Rohstoffe
Bi	Bismut
B_n	layer admittance
C	concentration
C_0	element concentration at ground
C_H	element concentration in presence of vegetation
CF	compact flash
ch	channel number
c_l	effective cable length
cps	counts per second
CPT	cone penetration testing
Cs	Cesium
©	copyright
d_a	apparent depth
D_a	apparent distance
DC	direct current
DEM	digital elevation model
DGPS	Differential Global Positioning System
DK	Denmark
DVD	Digital Versatile Disc
δ	inverse relative skin depth (= h/p)
δ_p	polynomial approximation of $\delta(\varepsilon_c)$

δ_T	residual (magnetics)
Δh_l	reduced laser altitude
ΔI	zero-level error of in-phase component
ΔQ	zero-level error of quadrature component
ΔT	anomalies of the total magnetic field
ΔT_f	anomalies of the total magnetic field, high-pass filtered
ΔV	diurnal (magnetic) variations
E	east
E	energy
E	ground level exposure rate
e	base of the natural logarithm (1/e ≈ 0.37)
eTh	equivalent concentration of Thorium
eU	equivalent concentration of Uranium
EM	electromagnetic(s)
ERDF	European Regional Development Fund
EU	European Union
ε	ratio of measured HEM components (= Q/I)
ε_c	ratio of calculated HEM components (= Q/I)
ε_0	permittivity of air: 8.854×10^{-12} As/Vm
ε_n	layer permittivity
f	frequency
F	IRGF
FAS	Fugro Airborne Surveys
FFT	Fast Fourier Transform
ft	feet
G	gain constant
GBA	Geologische Bundesanstalt
GPS	Global Positioning System
h	bird altitude
H	thickness of vegetation
HCP	horizontal coplanar
h_e	effective height
h_0	nominal survey height
HEM	helicopter-borne electromagnetic(s)
HMG	helicopter-borne magnetic(s)
HRD	helicopter-borne radiometric(s)
h_GPS	GPS-Höhe
h_l	laser altitude
h_r, h_r	radar altitude
Hz	hertz
i	counter

I	in-phase component (real part) of the HEM data
I_c	calculated in-phase value
IAEA	International Atomic Energy Association
IAGA	International Association of Geomagnetism and Aeronomy
IGRF	International Geomagnetic Reference Field
J_0	Bessel function of first kind and zero order
K	degree Kelvin
K	Potassium
keV	kilo electron volts
kg	kilogram
kHz	kilohertz
km	kilometre
km/h	kilometres per hour
l	litre
log	logarithm
λ	wave number
m	metre
MeV	mega electron volts
μ	attenuation coefficient (vegetation or height)
μ_0	permeability of air:$4\pi \times 10^{-7}$ Vs/Am,
μ_n	layer permeability
µR/h	microroentgens per hour
n	number of frequencies
N	north
n, N	raw, corrected count rate
NaI	sodium iodide
NASVD	noise adjusted singular value decomposition
NL	non-linear
NL	The Netherlands
nT	nanotesla
$N_{m'}$	observed count rate at STP effective height
N_S	corrected count rate at nominal survey height
N_x	background and STP corrected count rates (x = K, U, Th)
$N_{x(corr)}$	stripping corrected count rates (x = K, U, Th)
Ωm	ohm metre (Ohm*m)
p	skin depth
P	barometric pressure
P_0	barometric pressure at sea level
PDF	Portable Document Format
ppm	parts per million
π	Pi (=3.14159265…)

Q	quadrature or out-of-phase component (imaginary part) of the HEM data
Q_c	calculated quadrature value
r	distance parameter
R_1	reflexion factor
r_l	conversion factor
ρ	resistivity
ρ_0	resistivity of air: > 10^8 Ωm
ρ_a	apparent resistivity
S	south
S	sensitivity
s	second
STE	standard error
STP	standard pressure and temperature
t	thickness (of a model layer)
t	time variable
T	air temperature
T_0	temperature at freezing point of water on Kelvin scale
T, TMI	total magnetic field intensity
tanh	hyperbolic tangent
TC	total count rate
Th	Thorium
Tl	Thallium
t_l	life time
T_{LP}	low pass cut-off period
U	Uranium
USA	United States of America
USB	Universal Serial Bus
UTC	Coordinated Universal Time
UTM	Universal Transverse Mercator Projection
V	volt
VCX	vertical coaxial
VRS	vertical resistivity section
W	west
WFD	Water Framework Directive
WGS	World Geodetic System
ω	circular frequency
X, Y, Z	Cartesian coordinates, Z depth axis
Z	relative secondary magnetic field
z*	centroid depth

1. Summary

Climate change simulations indicate a sea-level rise and increasing rainfall in the North Sea region leading to higher groundwater levels and a forced outwash of nutrients and pollutants from industrial areas, agriculture and landfills. CLIWAT (climate & water) is a transnational Interreg project in the North Sea region funded by the European Union with partners from Belgium, The Netherlands, Germany and Denmark. The goal of the project is to determine the effects of a possible climate change on groundwater systems, surface water and the freshwater/salt-water boundary in the North Sea and Baltic Sea region.

Geological and geophysical measurements were carried out in the seven pilot areas of the project. In order to map the existing groundwater structures with airborne geophysical methods the German Federal Institute for Geosciences and Natural Resources (BGR) conducted four surveys in Zeeland, Friesland (both NL) and Vojens (DK). One of these pilot areas covers parts of Northern Friesland. The aim of the airborne survey in this pilot area was to map the depth to the salt water and to outline lithological units being relevant for groundwater modelling.

By request of the Dutch project partners (Deltares/TNO, VITENS, Provincie Fryslân, Wetterskip Fryslân) a helicopter-borne survey of the area between Leeuwarden, Franeker and the North Sea coast was conducted by the BGR airborne group in August 2009. The airborne survey comprises a 5–10 km by 12–24 km wide area ranging from 5°26'E to 5°49'E and 53°11'N to 53°19'N. With 6 survey flights 41 ENE–WSW profile lines and 8 NNW–SSE tie lines were flown, totalling about 616 line-km. The nominal flight-line spacing was 250 m for the profile lines and 2000 m for the tie lines. Due to a radar station for air-traffic control strongly affecting the airborne measurements, an area of about 7 km by 10 km in the centre of the planned survey area could not be covered by the airborne survey.

The BGR helicopter-borne geophysical system includes six-frequency electromagnetics (HEM), magnetics (HMG) and radiometrics (HRD). The electromagnetic system provides information about the distribution of electrical conductivity in the earth down to a maximum depth of 150 m. The intensity of the earth's total magnetic field is measured with a magnetometer. Magnetic anomalies may have deep sources as well as shallow ones. The intensity of the gamma radiation is registered by a gamma-ray spectrometer. The radiation measured is mainly emitted from the elements thorium, uranium, and potassium. The origin of this radiation is normally close to the earth's surface.

The helicopter-borne system consists of the BGR helicopter, the geophysical equipment and electronic equipment for navigation. The HEM and HMG sensors, a GPS antenna and a laser altimeter are installed inside a towed tube, called bird. The navigation instruments and the gamma-ray spectrometer are mounted in the helicopter. A ground base station records the time-variant data required to correct the airborne data.

The survey altitudes of the sensors are normally 30–40 m for electromagnetics and magnetics and 70–80 m for gamma-ray spectrometry. HEM and HMG data are recorded 10 times per second during a survey flight and HRD data are recorded once per second. At an aircraft speed of about 140–150 km/h, this leads to mean sampling intervals of about 4 m and 40 m, respectively.

The collected geophysical data and the corresponding positioning data are stored on a CF card during the flight. The digital data are checked immediately after the flight. Further processing of all survey data, including the data of the simultaneously operating base station which records the variations of the total magnetic intensity and the variations of the atmospheric pressure, take place in the field and finally at BGR in Hanover.

This "Technical Report" describes the survey operations and the survey equipment used, as well as the data processing and the presentation of the results as vertical resistivity sections and thematic maps. The processed data, the thematic maps and the vertical sections are stored on a DVD, accompanying this report.

Following parameters are displayed on two topographic map sheets (SW and NE) at a scale of 1:25,000:

- actual flight lines,
- topographic elevations,
- apparent resistivities at six frequencies (387, 1,821, 5,405, 8,388, 41,460 and 133,300 Hz),
- centroid depths at six frequencies (387, 1,821, 5,405, 8,388, 41,460 and 133,300 Hz),
- resistivities at 2, 4, 6, 8, 10, 15, 20 and 25 m below ground level,
- anomalies of the total magnetic field,
- concentration of potassium,
- equivalent concentration of thorium,
- equivalent concentration of uranium,
- total count rate,
- exposure rate.

Cross-sections based on resistivity-depth 1-D inversion models (vertical resistivity sections) are displayed along all flight lines at a horizontal scale of 1:25,000 with a vertical exaggeration of 25.

2. Introduction

Climate change simulations indicate a sea-level rise and increasing rainfall in the North Sea region. This will lead to higher groundwater levels and a forced outwash of nutrients and pollutants from industrial areas, agriculture and landfills (http://cliwat.eu/). The climate changes will affect the assessment of suitable industrial and agricultural development areas due to changes in the shape of the local waterworks catchments areas. Rise in groundwater level will challenge the construction business and it will be necessary to come up with new standards. It will also change the available groundwater resource and pattern of stream flow between summer and winter (reduced potential for irrigation from water table aquifers interacting with streams).

CLIWAT (climate & water) is a transnational project funded by the Interreg IVB North Sea Region Programme of the European Regional Development Fund (ERDF) with partners from four participating countries of the European Union (EU): Belgium (Ghent University), The Netherlands (Deltares/TNO, VITENS, Provincie Fryslân, Wetterskip Fryslân), Germany (LIAG, LLUR, SEECON, BGR) and Denmark (Region Midtjylland, GEUS, Region Syddanmark, Environment Centre Aarhus, Environment Centre Ribe, Aarhus University, Municipality of Horsens).

The goal of the project is to determine the effects of a possible climate change on groundwater systems, surface water and the freshwater/salt-water boundary in the North Sea and Baltic Sea region. The effect of the increased flux from agricultural and industrial land sites and landfills on groundwater quality in relation to indicators in the EU Water Framework Directive (WFD) has to be investigated as well as the impact on waterworks and important ground water aquifers near the coastlines. Also open question are the potential towards more accessible water in the hydrological system, the assessment of the consequences due to the increased recharge to groundwater systems and how to manage and solve the upcoming challenges for the construction business, for drainage and changes in conditions for biological/chemical decomposition in the soil.

Therefore geological and geophysical measurements were carried out in the seven pilot areas of the project (**Fig. 1**):

A: Belgische Middenkust, Belgium,

B: Zeeland, The Netherlands,

C: Terschelling and Northern Friesland, The Netherlands,

D: Borkum, Germany,

E: Schleswig and Southern Jutland, Germany and Denmark,

F: Egebjerg, Denmark,

G: Aarhus river, Denmark.

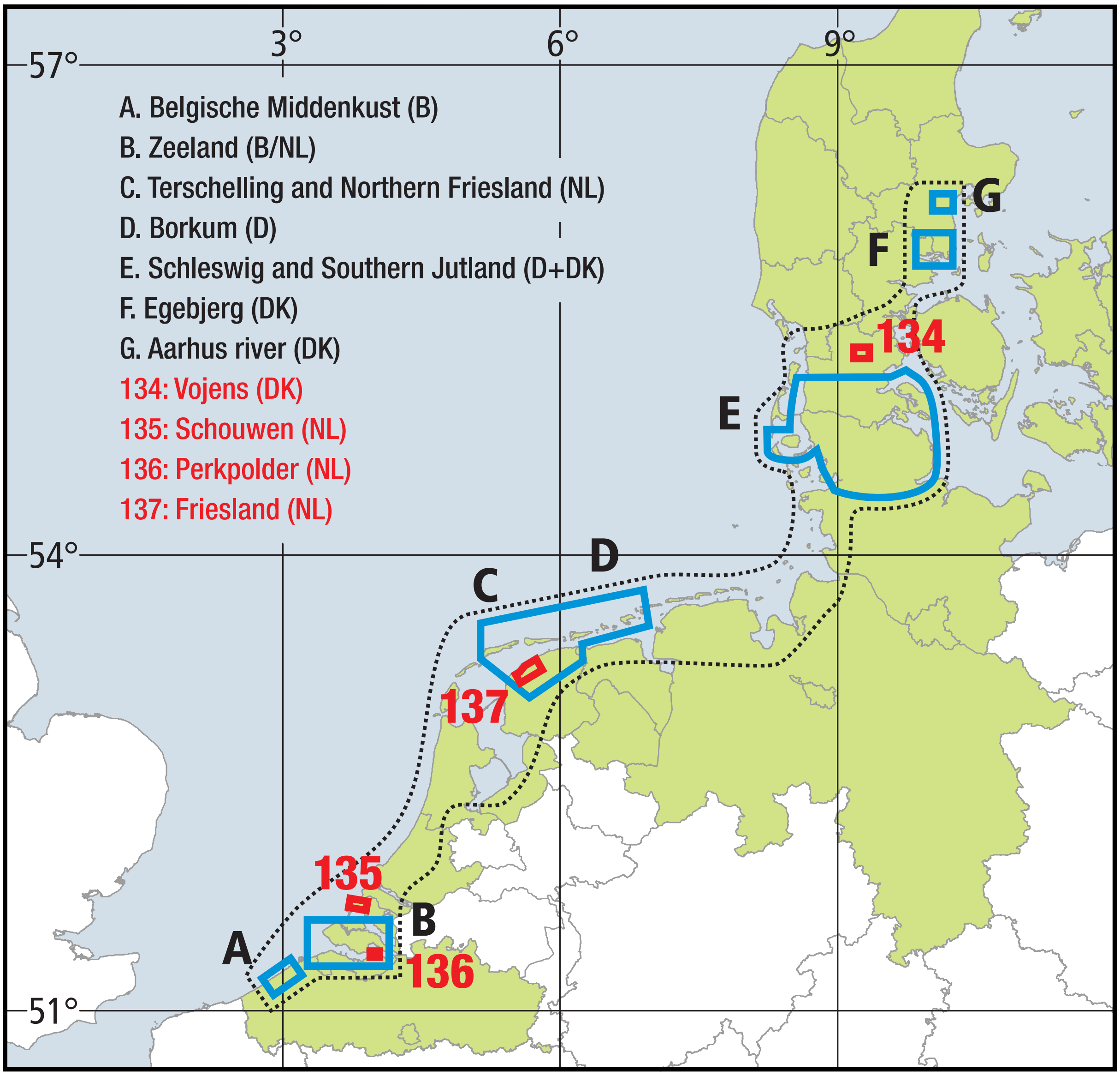

Fig. 1: *Regions (green) funded by the Interreg IVB North Sea Region Programme of the European Regional Development Fund (ERDF) and project areas A-G. Red numbers indicate the BGR airborne survey areas.*

One of these pilot areas (**C**) covers parts of Northern Friesland (**Fig. 2**). The aim of the airborne survey in this pilot area was to map the depth to the salt water and to outline lithological units being relevant for groundwater modelling.

A helicopter-borne survey of the area between Leeuwarden, Franeker and the North Sea coast was conducted by the BGR airborne group in August 2009. The Dutch project partners, who are responsible for the coordination of the measurements and the interpretation of the diverse data sets of the area, requested this airborne survey.

This "Technical Report" describes the survey operations and the survey equipment in use, as well as the data processing and the presentation of the results as vertical resistivity sections and thematic maps. The processed data, the thematic maps and the vertical sections are stored on a DVD accompanying this report.

3. Survey Area

The Friesland survey area is bounded by the towns of Leeuwarden and Franeker in the south and the North Sea coast in the north. It comprises a nominally 7–9 km by 12–19 km wide area. The actual survey area ranging from 5°26'E to 5°49'E and 53°11'N to 53°19'N differs from the planned one due to a radar station for air-traffic control strongly affecting the airborne electromagnetic measurements. Thus, an area of about 7 km by 10 km in the centre of the planned survey area could not be covered by the airborne survey. Instead the survey area was extended to the west, south and east. A map of the projected survey area (small red dots) and its actual realization (bold red dots) is shown in **Fig. 2**, which also shows the boundary (dashed grey lines) of the two 1:25,000 topographic map sheets used to present the geophysical results.

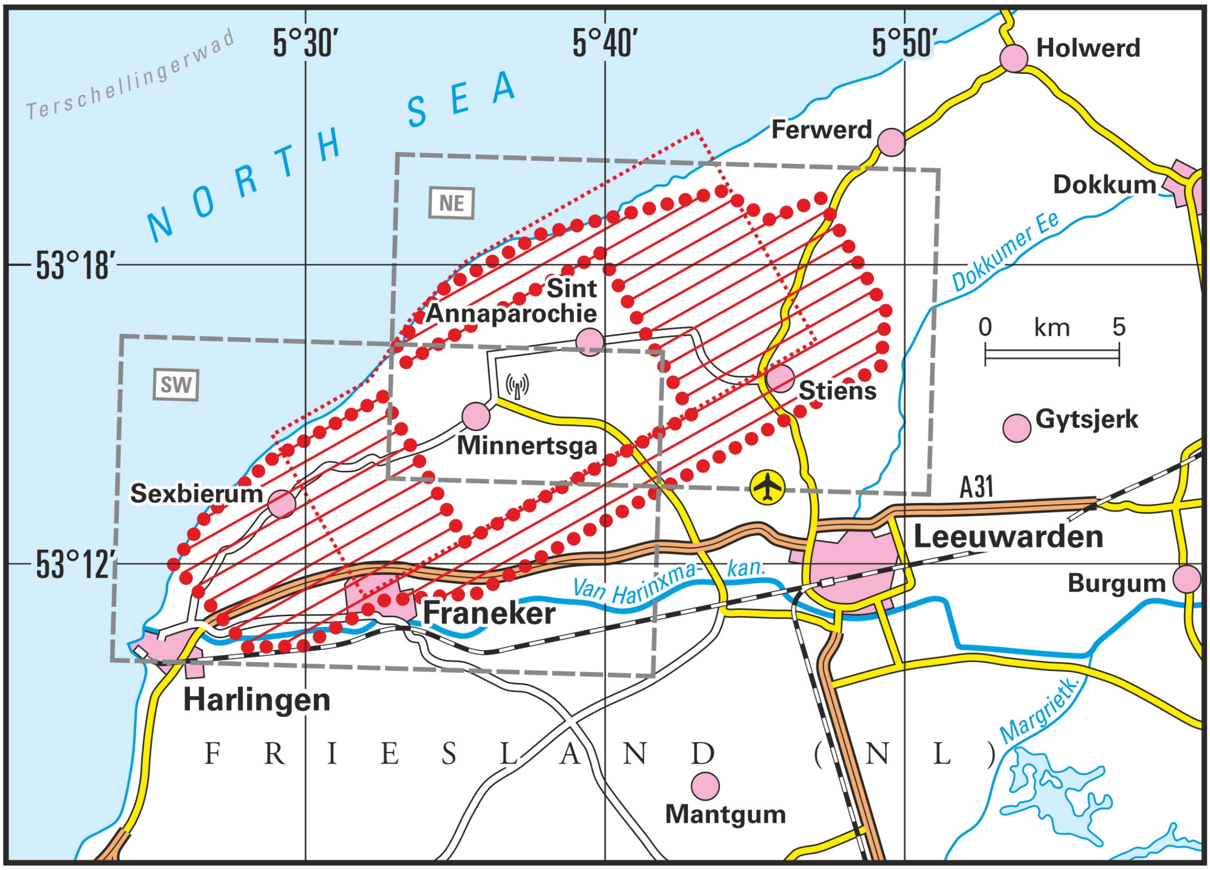

Fig. 2: *Friesland survey area (bold red dots), projected area (red dotted line) and the frame of the map sheets (grey dashed lines).*

An area of approximately 162 km² was surveyed with 6 survey flights on August 18–20, 2009. There were 41 ENE–WSW profile lines and 8 NNW–SSE tie lines flown, totalling about 616 line-km. The nominal flight-line spacing was 250 m for the profile lines and 2000 m for the tie lines. The survey flights commenced from Leeuwarden airport (0 m asl). The survey parameters are given in **Table 1**.

Table 1: *Survey parameters for the Friesland survey area.*

Survey area BGR area number	Friesland (NL) 137
Field period	August 18–20, 2009
Size of survey area	162 km²
Total length of survey lines	616 km
Number of survey flights	6 (+3)
Flight numbers	13701–13709(21)
Mean flight altitude of the EM sensor above ground	35 m
Mean survey speed	126 km/h
Number of profile-line flights	5 (+2)
Number of profile lines	67
Profile-line lengths	4–21 km
Profile-line directions (angle to N)	58°
Profile-line spacing	250 m
Number of tie-line flights	1 (+1)
Number of tie lines	8
Tie-line lengths	5–10 km
Tie-line directions (angle to N)	-32°
Tie-line spacing	2000 m

Due to disturbances by the radar station the data acquisition system had to be rebooted during three survey flights, the flight lines 12–35 had to be split into an eastern and western part and tie lines 6–9 could not be flown. During HEM data processing four survey flights were split further and renamed (13710–13721). The lines flown primarily northwards or eastwards are normally given an even profile number, while the ones flown in the opposite directions are odd numbered. The profile lines have the extension ".1" (after the profile number) or ".3" (or ".4" for repeated lines), and the tie lines have the extension ".9". Details of the survey flights are given in **Appendix I**.

The average altitude of the helicopter was 35 m above ground level within the survey area. During a survey flight, particularly before the first and after the last profile, the altitude was increased to >350 m to check the calibration of the HEM system far from any disturbing influences.

The base station recording the magnetic variations was located on the airport Leeuwarden at 5°45'32''E, 53°13'49''N and 0 m asl.

4. Airborne Geophysical System

BGR's airborne geophysical system simultaneously records the electromagnetic, magnetic, and gamma-ray spectrometry data. The geophysical instrumentation, the navigation and positioning systems, the digital recording units, as well as other equipment needed for the survey flights are integrated in one measuring system carried by a Sikorsky S-76B helicopter (**Fig. 3**).

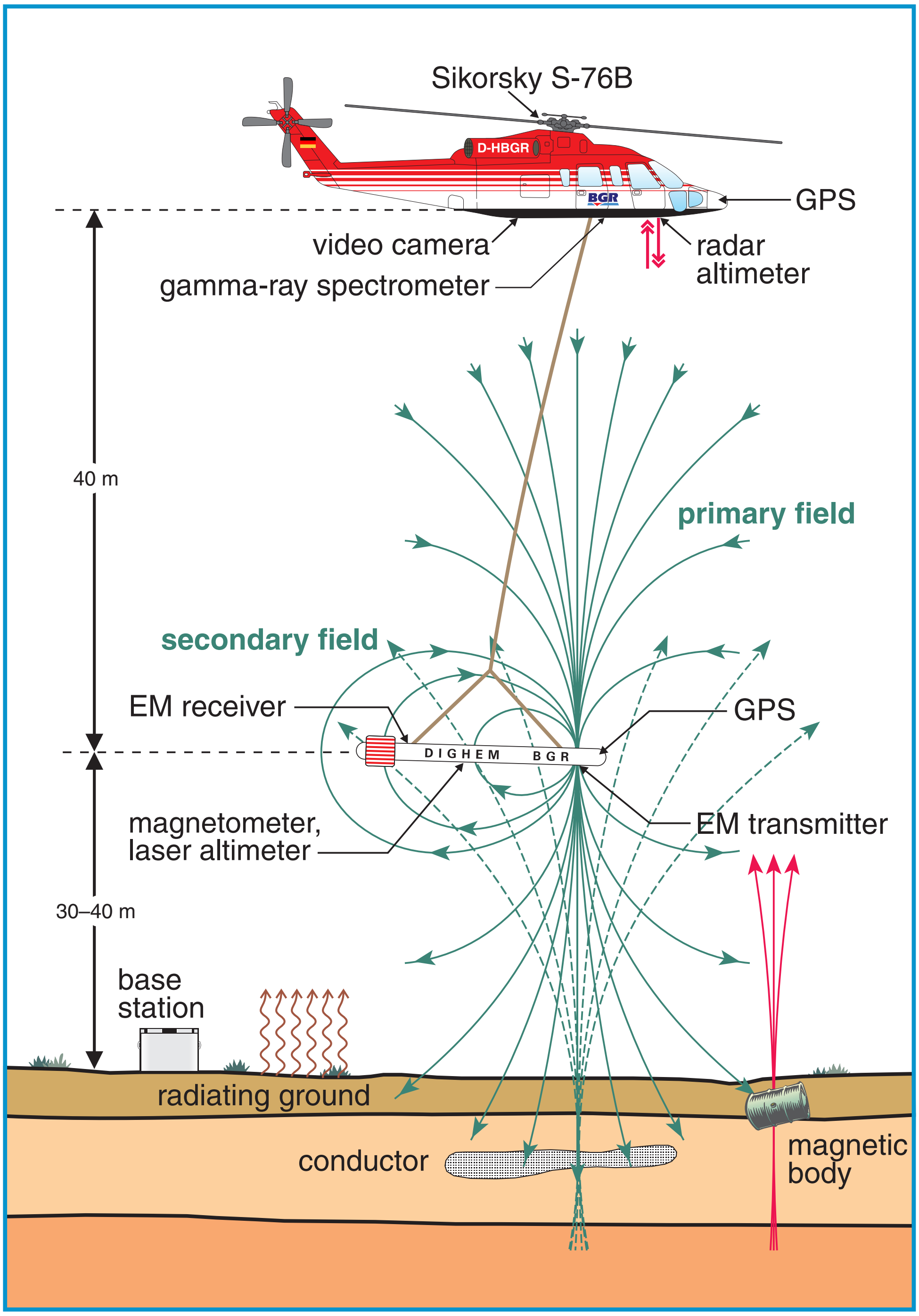

Fig. 3: *Principal sketch of the BGR airborne geophysical system.*

4.1. The Helicopter

The helicopter, a Sikorsky S-76B (see **Table 2**), was purchased in 1986 by the Federal Ministry for Economic Cooperation and Development and assigned to BGR, mainly for technical cooperation projects.

Table 2: *Technical specifications of the BGR helicopter D–HBGR*

Helicopter	
Type	Sikorsky S-76B (Manufacturer: Sikorsky, USA)
Year of manufacture	1986
Engines	2 turbines Pratt & Whitney PT6B-36A with 1033 SHP (shaft horse power) for each
Maximum gross weight	11,700 pounds (5,363 kg)
Maximum payload	3,300 pounds (1,500 kg)
Maximum flight duration	2:45 hours
Fuel consumption per hour	350–400 l

4.2. Measuring System

The airborne geophysical system (**Table 3**) is installed in the helicopter and in a towed tube, called bird. The navigation instruments and the gamma-ray spectrometer are mounted in the helicopter. The HEM and HMG sensors, a GPS antenna and a laser altimeter are installed inside the bird. This bird is towed by a 45 m long cable and its position is, depending on the flight speed, about 40 m beneath and little behind the helicopter. A ground base station records the time-variant data required to correct the airborne data.

The geophysical and recording systems are controlled by the HeliDas system that also assists navigation during a survey flight. The operator and the navigator are able to check the flight data online as information about the flight path and selected data channels are displayed on tablet computers.

Table 3: *The geophysical survey system*

Geophysical systems		
Bird	**I. Six -frequency electromagnetic system (HEM)**	
	Function	Investigation of the underground electric conductivity down to a maximum depth of about 150 m
	Manufacturer	Fugro Airborne Surveys (FAS), Canada
	Type	RESOLVE, BKS36a (Bird 61)
	II. Caesium magnetometer	
	Function	Recording of the total magnetic intensity of the earth
	Manufacturer	Geometrics, USA
	Type	G-822A
Helicopter	**III. Gamma-ray spectrometer**	
	Function	Recording of the energy spectrum of natural and man-made gamma radiation within a range of 0 to 3 MeV
	Manufacturer	Exploranium, Canada
	Type	Spectrometer: GR-820; Detector crystals: GPX-1024/256

4.3. Electromagnetics

A sinusoidal current flow through a transmitter coil at a discrete frequency generates the primary magnetic field. At a distance greater than about 2 m this field is very similar to a field of a magnetic dipole located in the centre of the transmitter coil. The resulting eddy currents in the subsurface generate a secondary magnetic field that depends on the frequency used and the conductivity distribution. The difference of the fields picked up by the receiver coil and a bucking coil, which is used to cancel out the dominating primary field, is related to the primary magnetic field at the receiver coil, i. e., the quantity measured is the relative secondary magnetic field in parts per million (ppm). Due to a small phase shift between the primary and the secondary field, the relative secondary magnetic field is a complex quantity with in-phase and out-of-phase (quadrature) components.

The HEM system (RESOLVE) manufactured by Fugro Airborne Surveys utilises six individual coil systems consisting of transmitter, receiver, bucking and calibration coils. The transmitter and receiver coils have a diameter of about half a metre and a distance of about 8 m. The orientation of five transmitter-receiver coil systems is horizontal coplanar (HCP) what is suitable for groundwater exploration purposes as the induced currents are predominantly flowing horizontally resolving layered structures best. In addition, a vertical coaxial coil (VCX) system is used in order to better locate vertical structures such as fault or fracture zones. The coil systems are housed by a 10 m long tube.

Table 4: *HEM system parameters (Bird 61)*

Frequency [Hz]	Coil separation [m]	Coil orientation	Denotation FAS	Denotation BGR
387	7.938	horizontal coplanar	EM_3	1. frequency
1,821	7.931	horizontal coplanar	EM_5	2. frequency
5,405	9.055	vertical coaxial	EM_6	3. frequency
8,388	7.925	horizontal coplanar	EM_2	4. frequency
41,460	7.912	horizontal coplanar	EM_1	5. frequency
133,300	7.918	horizontal coplanar	EM_4	6. frequency

Small coils placed in the centre of each receiver coil are used for calibration. The calibration factors necessary to convert the measured signals to ppm values were provided by the manufacturer. The in-phase and quadrature components of the relative secondary magnetic fields are used to derive the three-dimensional distribution of the electrical conductivity – or its inverse, the resistivity – in the subsurface. Horizontal resolution and vertical resolution are achieved by moving the system and using different system frequencies, respectively. Due to the skin-effect (high frequency currents are flowing on top of a perfect conductor) the penetration depths of the electromagnetic fields increase with decreasing frequency and conductivity. The frequencies used range from 387 Hz to 133 kHz enabling exploration depth ranges of about 1–30 m in a very conductive host such as salt-water saturated sediments and 5–150 m in a rather resistive host such as freshwater saturated sandy sediments.

The HEM system is not only sensitive to the electrically conductive subsurface but also to anthropogenic objects like, e. g., buildings, metallic bodies, and electrical installations, which have influence on the data measured, particularly at lower frequencies. As the helicopter itself is such an object, the HEM system is towed at a sufficiently large distance (about 40 m) underneath the helicopter.

4.4. Magnetics

A highly sensitive caesium vapour magnetometer installed in the bird is used to measure the total intensity of the earth's magnetic field (unit Nanotesla, nT). The function of a caesium magnetometer is based on the measurement of the Larmor frequency that occurs in a special, optically pumped system in the sensor. The frequency is directly proportional to the magnetic field intensity and can be determined with high precision and accuracy. The resolution of the instrument is 0.01 nT.

The magnetic field measured is composed of different parts. The earth's main field, caused by sources in the earth's core, varies between approximately 20,000 nT in equatorial regions and 70,000 nT at the poles. It is superimposed by the crustal magnetic field caused by rocks containing magnetised minerals. These produce anomalies in the range between less than one and up to several hundred nT. In populated areas, anthropogenic sources such as buildings, industrial plants, power lines, etc. can produce additional locally confined and sometimes strong magnetic anomalies. Finally, the magnetic field is subject to temporal changes due to fluctuations in the state of the ionosphere and magnetosphere. These diurnal variations are in the order of several tens of nT.

In order to record the diurnal variations, a magnetic base station (**Table 5**) is operated. The station, also equipped with a caesium magnetometer, is installed close to the area of investigation at a magnetically undisturbed place. Data recorded by the base station during the survey are used to correct the total magnetic field measured during the flight. GPS time is used to synchronise both data sets.

Table 5: *Base station*

Base station	
Magnetic base station	
Function	Recording of the variation of the total magnetic intensity (TMI)
Manufacturer	Base station: FAS, Canada Magnetometer: Cs sensor H-8, SCINTREX, Canada
Type	CF1 Data Logger

4.5. Radiometrics

For geophysical investigations the count rates of the common terrestrial radioactive elements (or their isotopes and daughter products) Tl-208 (thorium series), Bi-214 (uranium series), K-40 (potassium) are of interest. Mapping of the distribution of these three elements in the ground are useful for geological investigations.

BGR uses a standard 256-channel spectrometer system consisting of four sodium iodide (NaI) crystals to detect the ground gamma radiation and one upward looking crystal to detect the radon radiation in the air. The spectrometer crystals are placed together in an aluminium box. Each crystal has a volume of approximately 4 l ($0.1 \times 0.1 \times 0.4$ m^3). Incident gamma radiation is absorbed by the crystals and transformed to light pulses that are converted to electric pulses using a photomultiplier tube. The amplitudes of the electric pulses are directly proportional to the energy of incident gamma radiation.

The spectrometer covers an energy spectrum from 0 to 3 MeV. Depending on their energy, the pulses are mapped into one of 255 energy channels. Channel 256 is reserved for recording cosmic radiation between 3 and 6 MeV. Spectra recorded by the system contain counts of gamma radiation collected and integrated over one second. Energy windows and channel ranges of the different radiation sources are listed in **Table 6**. The spectrometer is internally stabilised for possible drifts in gain. This is done independently for each of the four downward-looking crystals using the thorium peak. Shifts of the thorium peak (2.62 MeV) relative to the nominal value are identified and the gain of the photomultiplier tube of the respective crystal is corrected automatically. A caesium sample is used to stabilize the gain of the upward looking crystal.

Table 6: *Radiation sources and corresponding spectrometer parameters*

Radiation source	Energy window in MeV	Peak energy in MeV	Channel range
Total count	0.41–2.81	—	34–233
Potassium (K-40)	1.37–1.57	1.46	115–131
Uranium (Bi-214)	1.66–1.86	1.76	139–155
Thorium (Tl-208)	2.41–2.81	2.62	202–233
Cosmic radiation	3.0–6.0	—	255

4.6. Navigation and Positioning

The navigation system (**Table 7**) provides the pilot with all the information necessary to carry out a survey flight. Navigation software (LiNav, AG-NAV Inc.) calculates the coordinates of the starting and the end points of all survey lines from the coordinates of the corners of the survey area, the profile direction and the spacing of the flight lines. These coordinates are copied to the HeliDas system using a CF card or an USB stick. These profiles are displayed on the tablet computer with the line being flown highlighted.

Table 7: *Navigation and positioning systems*

<table>
<tr><th colspan="3">Systems for navigation and positioning</th></tr>
<tr><td rowspan="4">Helicopter</td><td colspan="2">Navigation system</td></tr>
<tr><td>Function</td><td>On-line determination and display of the GPS navigational data required by the pilot during a survey flight; recording of the geographic position of the helicopter and its altitude above mean sea level</td></tr>
<tr><td>Manufacturer</td><td>Navigation computer and display: FAS, Canada
GPS receiver: NovAtel, Canada</td></tr>
<tr><td>Type</td><td>Navigation computer: HeliDas
GPS receiver: NovAtel OEMV-2-L1/L2
GPS antenna: NovAtel L1/L2 ANT-532-e</td></tr>
<tr><td rowspan="4">Bird</td><td colspan="2">Positioning system</td></tr>
<tr><td>Function</td><td>Determination and recording of the geographic position of the HEM bird and its altitude above mean sea level</td></tr>
<tr><td>Manufacturer</td><td>Position recording and display: FAS, Canada
GPS receiver: CSI Wireless, Canada</td></tr>
<tr><td>Type</td><td>Position recording: HeliDas
GPS receiver: DGPS MAX</td></tr>
</table>

The pilot obtains all information required to fly the profiles as accurately as possible from a second display. The most important information is the lateral deviation from a line. The deviation appears digitally in metres, as well as on a bar diagram. The navigation computer receives information about the position of the helicopter from a GPS navigation receiver whose antenna is fixed outside on the helicopter. The error in the navigation data is less than 1–2 m.

The positioning system (**Table 7**) provides the coordinates of each geophysical measurement. A second GPS navigation receiver is used for this purpose, whose antenna is fixed inside the bird. The spatial positions of the sensors are determined from this positioning data. The error of the coordinates is also in the order of 1–2 m.

A radar altimeter (**Table 8**) attached to the bottom of the helicopter determines its altitude above the ground or above obstacles (e. g., large stands of trees and buildings) with a precision of ±3 m. The altitude is needed to process the radiometric data. A barometric altimeter is used to determine the altitude of the helicopter above mean sea level, but this altimeter is employed only as a backup for the GPS receivers. Without a base station as reference the GPS measurements may have an error of some metres.

The altitude of the bird above the ground must be accurately known for the processing of the electromagnetic data and to generate a digital terrain model. A laser altimeter (**Table 8**) inside the bird provides this altitude with a precision of ±0.2 m. A further advantage of the laser altimeter, in addition to its precision, is the focused laser beam allowing, compared to the radar altimeter, mostly better measurements of the true distance to the surface as it is less affected by the tree canopy.

Table 8: *Altimeters*

Altimeters		
Helicopter	**Radar Altimeter**	
	Function	Recording of the altitude of the helicopter above ground level
	Manufacturer	Sperry, USA
	Type	AA-200
	Barometric Altimeter	
	Function	Recording of the altitude of the helicopter above mean sea level
	Manufacturer	Rosemount, USA
	Type	1241A5B
Bird	**Laser Altimeter**	
	Function	Precise recording of the altitude of the HEM bird above ground
	Manufacturer	Riegl, Austria
	Type	LD90-3800VHS

The digital elevation model is derived from the GPS elevation of the HEM bird in m asl minus the laser altitude. Without a base station as reference for the GPS measurements, and thus, the topographic elevations may have an error of some metres.

4.7. Data Acquisition and Recording

The HeliDas system stores all the data digitally on CF card during a survey flight (**Table 9**). The data sets are ready for processing with GEOSOFT OASIS montaj. The most important data channels are also displayed on the tablet computers to enable continual checking of the data during the flight. Immediately after a flight, the digital data are copied to a field computer and checked more accurately in order to obtain an impression of the geophysical results and to detect any problems with the survey system.

Table 9: *Data acquisition and recording systems*

	Data acquisition and recording systems	
Helicopter	**Function**	Digitizing of the analogue signals, buffering of all digital data; flight path and displaying of selected data channels; storage of position and field data on CF card ready for processing with GEOSOFT OASIS montaj
	Manufacturer	FAS, Canada
	Type	HeliDas

4.8. Video System

A video camera (**Table 10**) is mounted in the bottom of the helicopter. Two monitors, one in the cockpit and one in the operator's rack, allow monitoring of the bird at take-off and landing as well as during the flight.

The video recording of the flight path is used to locate sources of anomalous or disturbed data on the ground. The flight path video can be correlated directly with the digital data.

Table 10: *Video system*

	Video system	
Helicopter	**Function**	Recording of the flight track and monitoring of the movements of the HEM bird during take-off, landing and flight
	Manufacturer	Colour camera: Sony, Japan Video recorder: AXI, Sweden
	Type	Colour camera: DC372P Video server: AXIS 241S

4.9. Additional Equipment

The 28 V DC on-board voltage of the helicopter is smoothly buffered by a 24 Ah battery and connected to a central power unit. From there it is distributed to the individual components of the system with built-in fuses to protect devices from overvoltage.

Control and recording units of the airborne geophysical system are mounted in a 19" rack. Shock absorbers between the base of the rack and a wood board which is firmly screwed to the floor of the helicopter minimize the transfer of vibrations originating from the rotor.

Table 11: *Additional equipment*

Additional equipment		
Helicopter	**Central power unit**	
	Function	28 V DC on-board voltage of the helicopter buffered by a 24 Ah buffer battery and connected to a central power unit
	Manufacturer	Sikorsky, USA
	Instrument rack	
	Function	19" rack on shock absorbers to mount all components of the airborne geophysical system
	Manufacturer	Sikorsky, USA

5. Processing and Presentation of the Survey Data

The general objectives of the data processing may be summarized as follows:

- quality control of the measured data;
- conversion of the field data into physical parameters;
- presentation of the results as maps and vertical sections.

5.1. General Processing Steps

The airborne geophysical data are copied from the CF card to field computers directly after a survey flight in order to save the data and to check them for plausibility and correctness. Using the software GEOSOFT OASIS montaj, the primary field data processing steps are conducted automatically, followed by a pre-processing of all survey data in order to display preliminary results.

The final data processing starts with the processing of the position data:

- coordinate transformation;
- correction of altitude data of the helicopter and the bird.

The following processing steps are valid for all methods:

- removal of spiky data;
- reduction of high-frequency noise by digital filtering;
- conversion of the data to the desired geophysical parameters;
- fixing of the ends of the profiles for splitting the flights into profiles;
- merging the flight-line data sets to area data sets;
- levelling of the data;
- storage of the final survey data and geophysical parameters;
- production of maps and vertical sections (only HEM).

The field data processing and the calculation of the physical parameters for each method are described in more detail in the following chapters. GEOSOFT OASIS montaj is used throughout if not otherwise noted.

5.2. Position Data

5.2.1. Coordinates

The coordinates of the helicopter and the bird recorded during the survey flight refer to the WGS 84 geographic coordinate system. These geographic coordinates are transformed to local Cartesian coordinates. False coordinates are corrected und gaps are interpolated.

All survey results refer to UTM WGS 84 coordinates (3° meridian, zone 31N).

5.2.2. Radar Altitude

The radar altitude data measured in feet at the helicopter (h_r_{mess}) have to be transformed to metres above ground level (m agl). For the purpose of comparison with the laser altitude data of the bird (h_l), the radar altitudes are also referred to the bird altitude (h_r)

$$h\_r\ [m] = h\_r_{mess}\ [feet] \cdot 0{,}3048\ [m/feet] \cdot r_l - c_l\ [m],$$

where

h_r	=	adjusted radar altitude (unit: m agl),
h_r_{mess}	=	radar altitude (unit: feet) measured by the altimeter,
r_l	=	conversion factor (gradient),
c_l	=	effective cable length (offset).

For this, the effective cable length, i. e., the distance between the helicopter and the bird, has to be estimated and subtracted. The effective cable length can be derived from the differences of the GPS elevations of the helicopter and the bird. Alternatively, the effective cable length and the conversion factor r_l of laser and radar altitudes are obtained by linear regression.

For the correction of the radar altitude data r_l = 1.04 and c_l = 44 m were used.

5.2.3. Laser Altitude

The laser altimeter data representing the bird altitude – as well as the radar altimeter data – may have gaps and outliers which have to be corrected by elimination and interpolation procedures. The movement of the bird causes attitudes (pitch and roll) deviating from the normal case and, thus, laser altitudes which are normally higher than the actual bird altitude. The mean pitch angle of about 6° is corrected by applying the corresponding cosine function. The roll angle is generally not known. Thus, after identification by comparison with the radar altitudes of the bird, strongly affected laser altitudes have to be eliminated and interpolated afterwards.

The measurements of the laser altimeter data may be affected by the tree canopy or other reflectors. Thus, the distance between the bird containing the electromagnetic and magnetic systems and the ground level is often not correctly measured resulting in laser altitudes which are too low.

The affected laser altitudes (h_l) are corrected with the help of a combination of several checks and filter techniques (**Table 12**). The first step is to reduce the effect of strong gradients in the laser altitudes due to rapid changes in bird or topographic elevation. A base line derived by applying a low-pass filter to the laser altitude data is subtracted from the laser altitude data to calculate reduced laser altitude values (Δh_l). Remaining outliers are removed by applying a very short non-linear filfilter. In order to identify and eliminate those segments where trees or other obstacles exist, two procedures are applied to the reduced laser altitude data:

a) Noise filter, followed by non-linear and low-pass filters applied to the noise channel (Δh_l_{noise}), and a high-noise threshold of 0.4 m;
b) Maximum filter and difference threshold of 2 m of filtered (Δh_l_{max}) and unfiltered (Δh_l) data.

The gaps of eliminated data are filled in with slightly shifted maximum values representing the corrected reduced laser altitudes. As the maximum values may be too high, their levels are shifted to the levels on both side of each gap. Finally, the corrected values are low-pass filtered (Δh_l_{kor}) and the base line is added again to get the corrected laser altitude values (h_l_{kor}). This procedure is able to eliminate all effects caused by single or small groups of trees. The effect of broad and densely wooded areas, however, is not always removed sufficiently and has to be corrected manually.

Table 12: *Filter parameters for the removal of the tree-canopy effect in the laser altitudes*

Type of filter	Filter parameters	Channel
Low pass	Cut-off period: 5 s (≈ 200 m)	h_l
Non linear	Window length: 1 point (≈ 5 m), tolerance: 1.0	Δh_l
Noise (normal distr.)	Window length: 7 points (≈ 28 m)	Δh_l
Non linear	Window length: 3 points (≈ 15 m), tolerance: 1.0	Δh_l_{noise}
Low pass	Cut-off period: 1 s (≈ 40 m)	Δh_l_{noise}
Threshold	Cut-off value (Δh_l_{noise}): 0.4 m	Δh_l
Maximum	Window length: 21 points (≈ 84 m)	Δh_l
Threshold	Cut-off value ($\Delta h\_l_{max} - \Delta h\_l$): 2 m	Δh_l
Low pass	Cut-off period: 3 s (≈ 120 m)	Δh_l_{kor}

5.2.4. Topographic Elevation

The topographic relief (topo) derived by the difference of the GPS based bird elevation (h_GPS) and the corrected laser altitude (h_l_{kor})

$$\text{topo [m asl]} = \text{h\_GPS [m asl]} - h\_l_{kor} \text{ [m]}$$

is used to derive a digital elevation model of the survey area. As the tree-canopy effect causes laser altitudes which are too low, the topographic elevations are too high. Therefore, the topographic values are also useful to identify and manually correct the laser altitude for remaining tree-canopy effects, particularly if external topographic data as reference are available.

In order to remove line effects the topographic elevation data were levelled with respect to the digital elevation model provided by the project partner.

5.3. Processing of the Electromagnetic Data

The evaluation of the measured I and Q values (in ppm), i. e., the real part (in-phase or 0°-phase) and the imaginary part (out-of-phase, quadrature or 90°-phase) of the relative secondary field requires several processing steps:

- application of calibration factors;
- zero-level and drift correction;
- data correction;
- transformation to half-space parameters;
- correction of man-made effects;
- levelling;
- interpolation and smoothing
- inversion to resistivity models.

While the half-space parameters, apparent resistivity and the centroid depth, are individually derived from secondary field values for each frequency, the final resistivity models are calculated at each survey point by 1-D inversion of the data of all (or selected) frequencies.

5.3.1. Calibration of the HEM System

The HEM system was calibrated by the manufacturer (FAS) on highly resistive ground in Mountsburg Conservation Area, Canada. After adjusting the phase with the help of a ferrite rod, well-defined external calibration coils were used to derive the ppm values of the internal calibration coils. These calibration factors are used to convert the voltages measured during a survey flight to ppm values representing the secondary magnetic fields (**Table 13**).

Table 13: *Calibration factors of the HEM system*

Frequency [Hz]	Calibration factors FAS I [ppm]	Q [ppm]	Calibration factors BGR I [ppm]	Q [ppm]
387	-205.3	-205.3	-209.8	-210.8
1,821	-175.4	-174.7	-174.7	-174.3
5,405	76.6	76.8	81.9	81.2
8,388	-144.4	-144.2	-209.4	-198.8
41,460	-667.3	-665.2	-657.4	-664.9
133,300	-1404.2	-1406.4	-685.5	-911.0

At the beginning of each survey flight and at high flight altitude, phase and gain of the EM system are adjusted automatically for each frequency using internal calibration coils. Due to instrumental drift, the calibration has to be checked several times during the flight. The calibration signals caused by internal calibration coils are compared with known calibration signals and phase shifts and gain correction factors are applied to the data.

As a mutual coupling with the subsurface during the ground calibration procedure and technical changes of the system caused modified calibration factors, a flight over highly conductive North Sea water in February 2009 was used to check the calibration values. The evaluation of this data set yielded a set of phase and gain corrections being enormous particularly for the 8.3 and 133 kHz frequency data (**Table 13**).

A further check of the calibration factors during the Friesland and Zeeland surveys in August 2009 yielded an updated set of mean phase and gain corrections (normally < 1% gain and <0.2° phase, but for 133 kHz: 7,5° phase and 16% gain and for 41 kHz: 5% gain). In addition, several corrections of the phase and gain values were necessary for the highest frequency data due to the disturbances by the radar station.

5.3.2. Zero-Level and Drift Correction

The signals measured by the receivers may still contain some non-compensated parts of the primary fields generated by the transmitters. These so called zero levels may also have thermal drift. The zero levels of the HEM data are generally determined at high flight altitudes (>350 m) several times during a survey flight as the ground response is negligible at this altitude, i. e., the secondary field should be close to zero. Zero-level reference points are set at such high-altitude profile segments, preferably where the signal is not noisy. The zero level is obtained individually for each data channel by linear interpolation of the picked values at adjacent zero level reference points.

This procedure enables to remove the long-term, quasi-linear drift. Short-term variations, however, caused by temperature changes due to altitude variations, which occur particularly in the highest-frequency data, cannot be corrected successfully by this procedure. Therefore, additional reference points – also along the profiles at normal survey flight altitude – have to be determined where the secondary fields are small but not negligible. At these locations, the estimated half-space parameters are used to calculate the expected secondary field values, which then serve as local reference levels (Siemon, 2009). As this drift correction procedure is often not sufficient, statistical levelling procedures have to be applied in addition (see **Section 5.3.6**).

5.3.3. Data Correction

Noise from external sources (e. g., from radio transmitters, power lines, sferics, built-up areas, streets, railway tracks) is eliminated from the HEM data by appropriate filtering or interpolation. All those field values (I or Q) are automatically eliminated which fall below the relative standard error (rel. STE = STE/Mean) of the field values within a given data window. The field values are smoothed using a combination of non-linear (Naudy & Dreyer, 1968) and low-pass filters to exclude outliers and to suppress high-frequency noise, respectively. Due to frequency dependent data qualities the data channels are treated individually (**Table 14**).

Induction effects from buildings and other electrical installations (see **Section 5.3.5**) or effects from strongly magnetized underground sources are normally not erased from the data during the initial stage of data processing.

Table 14: *Filter parameters for HEM data processing*

Frequency [Hz]	Mean / STE [Values]	Threshold (I/Q) of rel. STE	NL filter Values/Tolerance	LP filter T_{LP} [Values]
387	75 / 25	0.05 / 0.05	20 / 3.0	40
1,821	75 / 25	0.05 / 0.05	20 / 2.0	30
5,405	75 / 20	0.05 / 0.05	10 / 2.0	30
8,388	75 / 15	0.05 / 0.05	10 / 2.0	30
41,460	75 / 15	0.05 / 0.05	5 / 2.0	30
133,300	75 / 15	0.05 / 0.05	5 / 2.0	30–50

5.3.4. Conversion of the Secondary Field Values to Half-Space Parameters

The relative secondary magnetic field Z = (I_c, Q_c) for a horizontal-coplanar (HCP) coil pair with a coil separation r is calculated at an altitude h above the surface and at a frequency f by (e. g. Ward & Hohmann, 1988)

$$Z = r^3 \int_0^\infty R_1\left(f,\lambda,\rho,\mu,\varepsilon\right) \frac{\lambda^3 e^{-2\alpha_0 h}}{\alpha_0} J_0(\lambda r)\, d\lambda$$

where $\alpha_0^2 = \lambda^2 - \omega^2\mu_0\varepsilon_0 + i\omega\mu_0/\rho_0$ with $\mu_0 = 4\pi \cdot 10^{-7}$ Vs/Am, $\varepsilon_0 = 8.854 \cdot 10^{-12}$ As/Vm and $\rho_0 > 10^8$ Ωm, J_0 is a Bessel function of first kind and zero order, and R_1 is the complex reflection factor containing the material parameters (electric resistivity ρ, magnetic permeability μ and dielectric permittivity ε) of the subsurface. This complex integral is evaluated numerically using fast Hankel transforms (e. g. Anderson, 1989, Johansen & Sørensen, 1979). A similar formula exists for a coaxial coil (VCX) configuration yielding smaller ppm values (VCX ≈ -0.25 ∗ HCP). Following Weidelt (1991) the reflection factor R_1 for a N-layer half-space model is derived by a recurrence formula

$$R_1 = \frac{B_1 - \alpha_0\mu/\mu_0}{B_1 + \alpha_0\mu/\mu_0}$$

with

$$B_n = \alpha_n \frac{B_{n+1} + \alpha_n \tanh(\alpha_n t_n)}{\alpha_n + B_{n+1}\tanh(\alpha_n t_n)} \quad n = 1,2,\ldots,N-1 \quad \text{and} \quad B_N = \alpha_N$$

$$\alpha_n = \sqrt{\lambda^2 - \omega^2\varepsilon_n\mu_n + i\omega\mu_n/\rho_n} \quad n = 1,2,\ldots,N$$

where ρ_n, μ_n, ε_n and t_n are resistivity, permeability, permittivity and thickness of the n^{th} layer, respectively (t_N is assumed to be infinite). As magnetic effects and displacement currents are negligible, i. e., $\mu_n = \mu_0$, and $\varepsilon_n = \varepsilon_0$ only resistivities and depths are taken into account (**Fig. 4**).

Calculated secondary field values I_c and Q_c (in ppm) are used to convert the calibrated measured values (I and Q) to the parameters of a homogeneous half-space (Siemon, 2001),

- apparent resistivity ρ_a [Ωm] and
- apparent distance D_a [m] from the sensor to the top of the conducting half-space,

individually for each frequency.

For this, the reduced amplitude $A'_c = (h/r)^3 \cdot A_c$ with $A_c = (I_c^2+Q_c^2)^{1/2}$ and the ratio $\varepsilon_c = Q_c/I_c$ are calculated for an arbitrary half-space as a function of the ratio $\delta = h/p$ of sensor altitude h and skin depth $p = 503.3 \cdot (\rho_a/f)^{1/2}$.

The half-space parameters are then derived for each pair of measured secondary field values from the functions $A'_c(\delta)$ and $\delta(\varepsilon_c)$ approximated by polynomials ($A'_p(\delta)$ and $\delta_p(\varepsilon)$):

$$D_a = r\,(A'_p(\delta_p(\varepsilon)/A))^{1/3} \quad \text{and} \quad \rho_a = 0.4\,\pi^2 f\,(D_a/\delta_p(\varepsilon))^2.$$

The calculated distance D_a may differ from the observed HEM sensor altitude (in m above ground level), i. e., the top of the conducting half-space model needs not to coincide with the surface of the earth as determined by the altimeter. The difference between the two quantities is defined as the apparent depth $d_a = D_a - h$. If d_a is positive, a resistive cover is assumed above the half-space. If d_a is negative, a conductive cover is assumed.

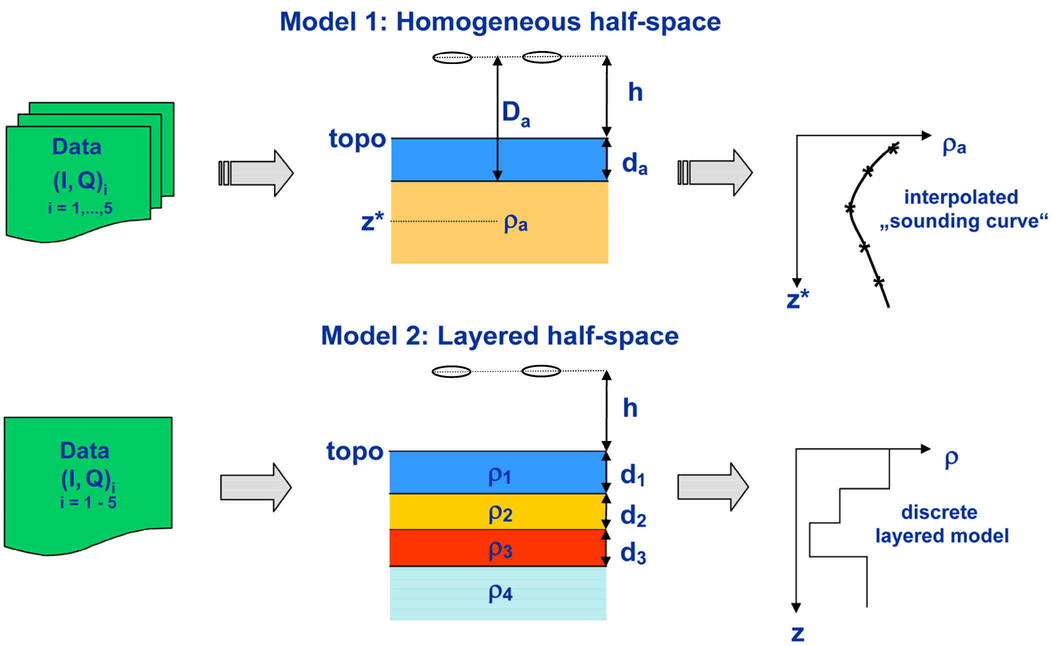

Fig. 4: *HEM inversion based on a homogeneous half-space or a layered half-space*

In addition to the apparent resistivity ρ_a and apparent distance D_a, the centroid depth $z^* = d_a + p/2$ is determined (Siemon, 2001). The centroid depth is a measure of the mean penetration of the induced underground currents. The resulting sounding curves $\rho_a(z^*)$ provide a initial approximation of the vertical resistivity distribution.
The actual approach for calculating the half-space parameters differs from that described by Siemon (2001) as the field values are calculated more accurately, particularly at higher frequencies, and the polynomial approximation of the functions $A'(\delta)$ und $\delta(\varepsilon)$ are optimised for each individual frequency.

The half-space parameters are checked for plausibility, i. e., high altitude (h > 100 m) and extreme (ρ_a > 1000 Ωm, d_a > 100 m) values have been eliminated before they are used for further processing.

5.3.5. Effect of Anthropogenic Influences on the HEM Data

In addition to the geogenic contribution to the secondary fields measured over densely populated areas, there is often an anthropogenic contribution from buildings and electrical installations etc. Generally, these have little influence on the HEM data and the data can be corrected using the standard data processing tools. In some cases, e. g., large buildings with a high metal content, the anthropogenic components in the HEM data are no longer negligible. Furthermore, external electromagnetic fields exist close to power lines, electric railway tracks or built-up areas which are able to substantially affect the HEM measurements. These man-made effects appear particularly in the lower frequency data because the geogenic contribution to the secondary fields is comparatively smaller at lower than at higher frequencies and, thus, the anthropogenic contribution, which is rather frequency independent, may dominate.

The anthropogenic influence lowers the calculated resistivity and associated depth. Thus, low resistivity and depth pattern on maps and sections often correlate with man-made effects such as villages or streets. These man-made effects can be detected in the HEM data due to their typical shape or by correlation with magnetic data. Topographic or Google Earth maps of the survey area, an analysis of the video records or an on-site inspection can help identify such effects.

A manual correction of man-made effects is very time consuming as each HEM channel of each survey line has to be examined individually. Therefore, a semi-automatic filter procedure has been developed and integrated into GEOSOFT OASIS montaj software. This procedure uses the gridded data of the half-space parameters apparent resistivity and apparent depth. These grids are inspected (once or several times) for anomalous data. Minimum and/or maximum anomalies are detected when the differences of the grid values and their corresponding median values, which are calculated in circular areas shifted over the grid, exceed a given threshold (**Table 15**).

Table 15: *Filter parameters for semi-automatic identification of man-made effects*

Frequency [Hz]	Radius [m] log ρ_a / d_a	Threshold log ρ_a / d_a	Number of passes log ρ_a / d_a	Type of anomaly log ρ_a / d_a
387	50 / 20	0.07 / 4	1 / 2	Min. / Both
1,821	50 / 40	0.12 / 3	1 / 1	Min. / Both
5,405	25 / 50	0.18 / 2	1 / 1	Min. / Min.
8,388	25 / 50	0.18 / 2	1 / 1	Min. / Min.
41,460	25 / 50	0.20 / 2	1 / 1	Min. / Min.
133,300	25 / 50	0.30 / 1.5	1 / 1	Min. / Min.

A topographic map and a Google Earth map are used to check whether the corresponding data segments are affected due to man-made sources and – if necessary – the data are reinstalled in manually selected areas. In order to close the remaining data gaps one can either apply gridding and resampling tools on the grids or use a spline interpolation along each survey line. Afterwards the HEM data are recalculated from the corrected half-space parameters. The measured HEM data are replaced by the calculated HEM data where the semi-automatic procedure has cut the data out.

5.3.6. Statistical Levelling

In order to identify and to correct zero-level errors in the HEM data a grid based micro-levelling (**Table 16**) is applied to the half-space parameters (log ρ_a and d_a) of the parallel survey lines. The resulting error grids are resampled along the survey lines and the smoothed (spline filter: smoothness = 1.0, tension = 0.5) error channels are subtracted from the half-space parameters.

Table 16: *Filter parameters for micro-levelling of log ρ_a and d_a*

Frequency [Hz]	Butterworth (high pass) Cut-off value, degree of filter log ρ_a / d_a	Directional cosine (pass) Azimuth, degree of function log ρ_a / d_a
387	800 m, 8 / 800 m, 8	148°, 1 / 148°, 1
1,821	800 m, 8 / 800 m, 8	148°, 1 / 148°, 1
5,405	800 m, 8 / 800 m, 8	148°, 1 / 148°, 1
8,388	800 m, 8 / 800 m, 8	148°, 1 / 148°, 1
41,460	800 m, 8 / 800 m, 8	148°, 1 / 148°, 1
133,300	800 m, 8 / 1000 m, 8	148°, 1 / 148°, 1

Strong HEM anomalies are normally smoothed by the two-dimensional lateral filtering of the micro-levelling procedure. Therefore, grids where the local anomalies have been removed beforehand are used for micro-levelling, resulting in rather smooth apparent resistivity and apparent depth maps.

The tie lines are levelled afterwards using the levelled line grids as reference. The smoothed (B-Spline filter, smoothness: 1.0, tension: 0.5) differences of levelled and unlevelled half-space parameters are used to correct the tie-line data.

The levelled half-space parameter values are then converted to secondary field values (I_c, Q_c) which are compared with the corresponding unlevelled values. Selected parts of the differences of the levelled and unlevelled values ($\Delta I = I - I_c$, $\Delta Q = Q - Q_c$) are strongly smoothed using a non-linear filter and a smoothing spline interpolation. The selection is based on constant (data noise, system altitude) and dynamic (I_{spline}, Q_{spline}) threshold values (**Table 17**). These interpolated smoothed differences are assumed to characterize the zero-level errors and they are used to correct the HEM data without losing details (Siemon, 2009). The levelling is done prior to the 1-D inversion of the HEM data.

Table 17: *Filter parameters for the levelling of HEM data*

Type of filter	Filter parameters	Channel
Threshold	Cut-off value (h_l_{kor}): 300 m	ΔI, ΔQ
Threshold	Cut-off value (I_{noise} , Q_{noise}): 0.05	ΔI, ΔQ
B-Spline	Smoothness: 1.0, tension: 0.2	I, Q
Non linear	Window length: 50 points (≈ 200 m), tolerance: 3.0	ΔI, ΔQ
B-Spline	Smoothness: 0.95, tension: 0.5	ΔI, ΔQ

5.3.7. 1-D Inversion of the HEM Data

The model parameters of the 1-D inversion are the resistivities ρ and thicknesses t of a layered half-space (**Fig. 4**), where the thickness of the underlying half-space is assumed to be infinite. Marquardt's inversion procedure is used (Sengpiel & Siemon, 2000), which requires a starting model. This starting model is derived from the apparent resistivity vs. centroid depth values $(\rho_a, z^*)_i$, i = 1,…,n (**Fig. 5**).

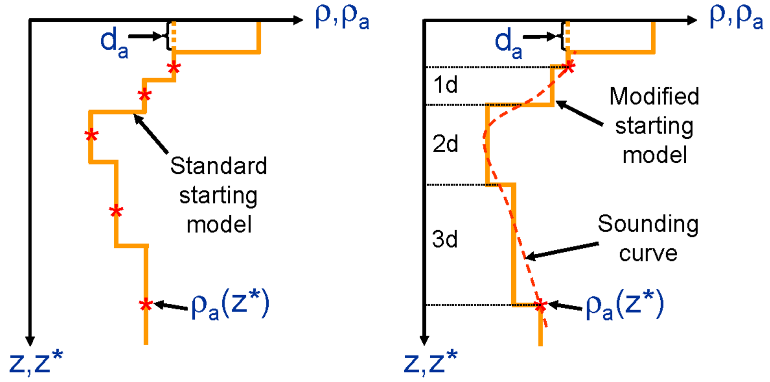

Fig. 5: *Construction of starting models derived from apparent resistivity ρ_a, centroid depth z*, and apparent depth d_a of a five-frequency HEM data set*

The standard starting model (Siemon, 2006) is constructed with respect to the number of frequencies used, i. e., the number of layers is given and the model layers correspond to the apparent resistivities and centroid depths of each frequency. The layer resistivities are set equal to the apparent resistivities, the layer boundaries are chosen as the logarithmic mean of each two neighbouring centroid depth values. The use of the standard starting model enables the highest resolution, but also the highest sensitivity to calibration errors. Therefore, a modified starting model is constructed having an arbitrary number of layers. The resistivities and depths of the first and last layers are derived from the apparent resistivities and centroid depths of the highest and lowest frequencies, respectively. These confining layer boundaries can be shifted upwards or downwards. The thicknesses of the intermediate layers increase linearly and the resistivities are picked from an apparent resistivity sounding curve at the corresponding layer centres (on a log scale). Optionally, a resistive cover layer may be used. The thickness of the cover layer is derived from the apparent depth

d_a of the highest frequency. If this apparent depth value is less than a minimum layer thickness value, the latter value (e. g. 0.5 m) is used.

As the laser altitude measurement are affected by the attitude of the HEM system resulting in measured bird altitudes that may be too high, the inversion may derive cover layers being to conductive. To overcome this difficulty, the bird altitude has to be variable. For this, a non-conducting cover layer is introduced representing a variable portion of the bird altitude. During the inversion the thickness of this layer (starting value: 5 m) is optimised.

The inversion procedure is stopped when a given threshold is reached. This threshold is defined as the differential fit of the modelled data to the measured HEM data. Normally a 10% threshold is used; i. e., the inversion stops when the enhancement of the fit is less than 10%.

The data of 5.5 kHz frequency were not used for inversion as they are obtained with a vertical coaxial coil system being sensitive to steeply dipping conductors (and also to external sources) whereas all others are obtained with horizontal coplanar systems.

The survey data were inverted with both types of starting models having five-layers and a non-conducting cover layer. A comparison with cone penetration testing (CPT) data showed that the use of the modified starting model provided the best results.

5.3.8. Presentation of the Results

The HEM results are presented on maps and vertical resistivity sections (VRS). The maps are produced for the half-space parameters, apparent resistivity and centroid depth, as well as for resistivities at eight depth levels (2–25 m below seal level) picked from 1-D inversion models. All the maps prepared from the results of this survey are listed in **Section 6.3**.

All data points used for the production of apparent resistivity and centroid depth maps are drawn as small black dots (flight lines). White dots mark areas of interpolated data. On the maps displaying resistivities at certain depths, the white dots inform about the number (frequencies) of interpolated data sets: the bigger the dot the more interpolated data were used for the inversion.

The VRS, also based on the 1-D inversion results, are produced for each of the survey lines. These vertical sections are constructed by placing the resistivity models (without a non-conducting cover layer) for each sounding point along a survey profile next to each other using the modelled topographic relief (i. e., the top of the conducting models) as base line (in m asl). For the purpose of comparison the measured topographic elevation is displayed by a black line. The thickness of the bottom layer (substratum) is derived from the corresponding resistivity, but the minimum thickness is 10 m. The altitude of the EM sensor, information about the data processing, the fitting error of the inversion, and the HEM data, which are described in a legend, are plotted above the resistivity models.

5.4. Processing of Magnetic Data

5.4.1. Magnetic Total Field

The earth's total magnetic field T at a point r and at a time t, e. g., measured with an airborne system, is the sum of the following parts:

$$T(r,t) = F(r) + \Delta V(t) + \Delta T(r) + \delta_T(r,t),$$

where

$F(r)$	=	geomagnetic main field (IGRF = International Geomagnetic Reference Field),
$\Delta V(t)$	=	diurnal variations of the earth's magnetic field,
$\Delta T(r)$	=	the crustal field in the survey area,
$\delta_T(r,t)$	=	anthropogenic part of the magnetic field.

The anomalies of the crustal field $\Delta T(r)$ caused by rock magnetization are of interest. While the IGRF $F(r)$, which can be calculated from table values, and the diurnal variations $\Delta V(t)$, which are recorded at the base station, can be subtracted from the measured total field, the anthropogenic part $\delta_T(r,t)$ cannot be quantified independently. Therefore, the derived ΔT values contain both the geogenic part and the disturbing anthropogenic part. Anthropogenic sources are located at the earth's surface (e. g., buildings, power lines, industrial sites). They are mostly locally constrained and thus can be identified using maps and other sources of information.

5.4.2. IGRF

The IGRF (International Geomagnetic Reference Field) can be calculated for any point on and above the earth's surface at a specific time on the basis of spherical harmonic coefficients, which are updated every five years by the International Association of Geomagnetism and Aeronomy (IAGA, 1992). The geomagnetic main field values of the survey area were calculated for each point using the IGRF-10 model from 2005 (IAGA, 2005).

5.4.3. Diurnal Variations

The base station for recording the time variant parts of the total magnetic field, the diurnal variations, was placed on the Leeuwarden airport at 5°45'32"E, 53°13'49"N and 0 m asl. $\Delta V(t)$ values are calculated as the measured value minus the IGRF value for the respective time and place. Possible disturbances of the base station recordings are eliminated using despiking and low-pass (filter width: 20) filters.

5.4.4. Levelling

After subtraction of the main field and diurnal variations from the measured magnetic field values, a statistical levelling is performed. The differences at the intersections of the flight lines and the tie lines are determined and averaged for each flight. The averaged values are then used to correct level errors that may occur in case of changes in the setup of the airborne or base station magnetic sensors during the survey.

Remaining, mostly small level errors may occur, inter alia, as result of different flight directions (heading errors) and are eliminated in a subsequent micro-levelling process. Micro-levelling is based on gridded line data in which level errors are identified using two-dimensional Butterworth high-pass (cut-off value: 1600 m, degree: 4) and directional cosine FFT (azimuth: 148°, degree: 1) filters. Result of the filtering process is an error grid which is sampled along the flight lines. The sampled error values are heavily smoothed using a B-Spline filter (smoothness: 1.05, tension: 0.5) and then subtracted from the original data. Gridding of the levelled data yields a ΔT grid that is virtually free of level errors. Finally, the tie-line data are fit to the levelled line-data grid by removing possible offsets and trends in their differences.

In (partly) populated areas, grids of ΔT values are mostly dominated by high-amplitude anthropogenic anomalies. These anomalies act as a source of disturbance during the micro-levelling process as well as during the identification of weak geogenic magnetic anomalies. Therefore, a semi-automatic filter procedure is applied to the data prior to micro-levelling. The procedure detects anomalous data in the ΔT grid. Anomalies are detected when the differences of the grid values and their corresponding median values, which are calculated in circular areas shifted over the grid, exceed a given threshold. Manual interaction in the detection process is possible. The resulting grid is, as far as possible, freed from anthropogenic anomalies and is used as input for the micro-levelling process. The anthropogenic regions blanked in the finally levelled data are re-introduced by applying error values interpolated from neighbouring data sections to them. The levelled data are used to produce a final ΔT grid based on all data including anthropogenic anomalies.

5.4.5. Presentation of the Results

The maps produced to display the magnetic anomaly data are listed in **Section 6.3**. All data points used for map production are drawn as small black dots (flight lines). White dots mark areas of interpolated data.

5.5. Processing of Gamma-Ray Spectrometry Data

The natural gamma radiation of rocks and soil is mainly generated by the radioelements potassium, uranium, and thorium. According to the recommendations of the IAEA (2003), the spectrometry data recorded in the aircraft have to be converted to equivalent ground concentrations of these elements. This requires some preparatory procedures regarding spectrometer calibration and a number of data processing steps listed below.

Spectrometer calibration:

- Determination of cosmic and aircraft background count rates by means of flights over extensive water bodies
- Determination of stripping ratios for Compton scattering correction using calibration pads
- Determination of height attenuation and sensitivity coefficients by means of flights over a calibration range
- Determination of vegetation attenuation coefficients

Data processing:

- Energy calibration
- Reduction of count rate statistical noise
- Determination of detector height above ground and effective height
- Live time correction
- Background correction
- Compton (stripping) correction
- Height-attenuation reduction
- Calculation of equivalent ground concentrations

5.5.1. Energy Calibration

The spectral stability of gamma spectrometers is not perfect. Due to temperature effects, the mapping of energy peaks to correct channel positions may drift slightly during a survey flight. Therefore, an energy calibration is applied to the recorded spectra during data post processing. The channel-energy mapping of a spectrometer can be expressed as follows:

$$ch = E / G + offs,$$

where

ch = channel number,
E = energy in keV,
G = gain constant of spectrometer in keV/channel,
offs = channel offset.

A 256-channel spectrometer has a nominal gain constant of 12.0 keV/channel and an offset of 0 channels. In order to determine the actual gain and offset of the spectrometer used, mean spectra are calculated for each flight line. The positions of the known energy peaks in the mean spectra (K, U, Th) can then be used to calculate actual gain and offset of the instrument during each of the analysed time windows (flight lines). Based on these values, the recorded spectra are re-mapped to a nominal 12 keV/channel raster.

5.5.2. Reduction of Statistical Noise

Due to a relatively large distance between the sources of radiation at the earth's surface and the radiation detector in the helicopter, count rates in airborne gamma-ray surveys are generally low. This results in a high portion of statistical noise present in the recorded spectra and, consequentially, also present in the calculated ground concentrations of radioelements. Therefore, a method for noise reduction developed by Hovgaard & Grasty (1997) is applied to the data. The NASVD method (noise adjusted singular value decomposition) is based on a statistical analysis of all spectra recorded in a survey area and a reconstruction of noise reduced spectra using singular value decomposition routines. The procedure results in smoothed spectra reconstructed from five principal components, from which the count rates for the energy windows of interest (see **Table 6**) are determined. Furthermore, an adaptive filter (Mathis, 1987) for smoothing the count rate channels (filter width: 10) is applied.

5.5.3. Detector Height above Ground and Effective Height

Knowledge of the distance between the source of radiation (on the ground) and the detector (in the helicopter) is crucial for inferring ground concentrations of radioelements from airborne radiometric data correctly. The helicopter system used by BGR is equipped with two altimeters: a radar altimeter in the helicopter and a laser altimeter in the EM bird. Generally, the radar altimeter data are used to determine the detector's height above ground because it is installed on the same platform. However, the data from the laser altimeter are more precise and also contain information on the presence and eventually the thickness of vegetation on the ground beneath the system. Whereas, in forested areas, the radar altimeter detects the tree canopy and underestimates the ground distance, laser altimeter data allow both for estimation of the true ground distance and the vegetation height, which is required for an application of a vegetation attenuation correction (see **Section 5.5.8**). Therefore, a fusion of data from the radar and laser altimeters is performed, resulting in a more accurate estimation of the detector height above ground and an estimation of vegetation height.

In order to apply the radiometric analysis techniques, it is necessary to convert actual environmental conditions of the survey to standard conditions. This includes the adjustment of the measured ground clearance to standard temperature and pressure (STP conditions). The adjusted ground clearance value called "effective height" has the same mass of STP air between the ground and the helicopter as the actual one during data acquisition. The adjustment is applied according to IAEA (2003):

$$h_e = (h_r \cdot P \cdot T_0) / (P_0 \cdot (T + T_0)),$$

where

h_e = effective height above ground level at STP [m],
h_r = helicopter height above ground, determined from corrected radar altimeter data [m],
T_0 = 273.15 K; freezing point of water on Kelvin scale,
T = air temperature [°C],
P_0 = 101.325 kPa; mean air pressure at sea level,
P = barometric pressure [kPa].

5.5.4. Live Time Correction

Gamma-ray spectrometers need a certain amount of time to process a pulse detected by the system. During that time, further incoming pulses are rejected. The amount of time the system is able to detect pulses ("live time") is recorded by the system. Due to the statistical nature of gamma radiation a correction of measured count rates in order to obtain count rate values for a nominal 1 s integration interval (IAEA, 2003) is easily achieved by the following formula:

$$N = n \cdot 10^3 / t_l,$$

with

- N = corrected count rate,
- n = raw count rate,
- t_l = system live time in milliseconds.

5.5.5. Background Radiation Correction

Cosmic radiation background is caused by high-energy (>3 MeV) cosmic ray particle interaction with the atmosphere. Another source of background radiation is the immanent radioactivity of the helicopter and its equipment. Background radiation distorts the measurements of geogenic radiation and has to be corrected for. The required correction coefficients are determined by means of flights over extensive water bodies at altitudes between 100 and 3500 m. The background correction is applied according to the following formula:

$$N = a + b \cdot C,$$

where

- N = combined cosmic and aircraft background for each channel,
- a = aircraft background for each channel,
- b = cosmic rate stripping factor for each channel,
- C = low-pass filtered cosmic channel (> 3 MeV) count.

The values a and b were determined using data from test flights at different altitudes over the North Sea in 2008. For each channel K, U, Th, and TC (total count) a linear regression of the count rates for different altitude intervals and the filtered cosmic channel count rates revealed values for a and b. The values are listed in **Table 18**.

Table 18: *Aircraft background and cosmic stripping factors*

Channel	Aircraft background a [cps]	Cosmic stripping factor b
TC	31.09	0.722
K	5.51	0.041
U	0.48	0.033
Th	0.33	0.041

5.5.6. Compton Correction

Compton scattering leads to certain amounts of radiation from one energy window being scattered into other energy windows. For example, some amount of thorium radiation will be scattered into lower energy windows such as uranium and potassium. The removal of these effects (Compton correction) is done using so-called stripping ratios. These coefficients describe the magnitudes of scatter between the energy windows of interest. They were determined in 2008 using portable calibration pads (Grasty et al., 1991) and are listed in **Table 19**.

Table 19: *Stripping ratios*

	Stripping ratio	Value
Th → U	α	0.2485
Th → K	β	0.3852
U → K	γ	0.6599
U → Th	a	0.0395

The values of α, β, γ increase with altitude of the helicopter above ground level and have to be corrected on the base of STP equivalent altitude according to the following factors (see IAEA, 2003):

$$\alpha_e = \alpha + 0.00049 \cdot h_e$$
$$\beta_e = \beta + 0.00065 \cdot h_e$$
$$\gamma_e = \gamma + 0.00069 \cdot h_e$$

with

h_e = equivalent height above ground level at STP in metres.

To obtain the net count rates of the particular energy windows, the stripping ratios are applied to the data:

$$N_{Th(corr)} = (N_{Th} - aN_U) / (1 - a\alpha)$$
$$N_{U(corr)} = (N_U - \alpha N_{Th}) / (1 - a\alpha)$$
$$N_{K(corr)} = N_K - \beta N_{Th(corr)} - \gamma N_{U(corr)}$$

where N_{Th}, N_K, N_U represent the background and STP corrected count rates, $N_{Th(corr)}$, $N_{U(corr)}$, $N_{K(corr)}$ are the stripping corrected count rates, and α, β, γ, a are the STP corrected stripping ratios. No Compton correction is applied to the total count values (see IAEA, 2003).

5.5.7. Height-Attenuation Reduction

The intensity of gamma radiation measured in airborne surveys varies approximately exponentially with height. In order to estimate count rates at a nominal survey height of 80 m, the following formula is used:

$$N_s = N_m \cdot e^{-\mu\,(h_0 - h_e)},$$

where

μ = window attenuation coefficient (per metre),
N_m = observed count rate at STP effective height h_e,
N_s = corrected count rate for the nominal survey height h_0.

The values (**Table 20**) were determined from data acquired at different heights over the Allentsteig (Austria) calibration range in 2003.

Table 20: *Height attenuation coefficients*

Window	Height attenuation coefficient µ (per metre at STP)
K	0.007733
U	0.008132
Th	0.005784
TC	0.006468

5.5.8. Radioelement Concentrations and Exposure Rate

IAEA (2003) recommends converting the count rates for the three radioelements into surface concentrations and exposure rates at ground level. The advantage is that the results of measurements with different instruments (e. g. with different crystal volumes) can be compared with each other. Conversion between count rates and concentrations is done using sensitivity coefficients (**Table 21**):

$$C = N_s / S,$$

with

C = element concentration (K in %, eU in ppm, eTh in ppm),
N_s = count rate for each window (after height attenuation and stripping),
S = broad source sensitivity for the spectral window.

The calculated concentrations are expressed as equivalent concentrations eU and eTh (in ppm) and as concentrations of K (in %).

Table 21: *Sensitivity coefficients*

Sensitivity
1 % K = 28.42 cps
1 ppm eTh = 1.96 cps
1 ppm eU = 2.92 cps

The sensitivities (**Table 21**) were determined over the Allentsteig (Austria) calibration range. Concentrations calculated this way refer to an infinitely extended and permanently radiating plane. They may differ from the actual concentrations of the elements at ground surface, especially in areas of irregularly distributed radiation sources and under wet conditions. Furthermore, the presence of atmospheric radon may vary considerably during a survey. Radon can spoil radiometric data, in par-particular uranium concentrations inferred from count rates, because radon and uranium radiation is detected in the same energy window. Presently, there is no correction of the effect of radon radiation on airborne gamma-ray measurements implemented in our radiometric data processing routines. Absolute values of uranium concentrations indicated in the maps are therefore to be regarded with caution.

The calculated concentrations will also be erroneous in areas where vegetation, mostly trees in forested areas, absorbs part of the radiation from the ground. A vegetation correction can be applied to the data assuming that the attenuation of gamma radiation varies exponentially with vegetation thickness and vegetation thicknesses are known:

$$C_H = C_0 \cdot e^{-\mu \cdot H},$$

where

C_0	=	element concentration at the ground,
C_H	=	element concentration determined in the presence of vegetation,
H	=	thickness of vegetation,
μ	=	linear attenuation coefficient of vegetation.

Values for μ (**Table 22**) were determined empirically using extensive data sets acquired over northern Germany. Vegetation thicknesses were inferred from laser altimeter data. In addition to the three radioelements, an attenuation coefficient for the total count energy window was determined empirically.

Table 22: *Linear attenuation coefficients μ for vegetation*

Element	μ
K	0.012
U	0.008
Th	0.011
TC	0.006

The ground level exposure rate is calculated as a function of the K, U, and Th concentrations after application of the vegetation correction:

$$E = 1.505 \cdot K + 0.653 \cdot eU + 0.287 \cdot eTh,$$

with

E	=	ground level exposure rate [μR/h]

using the following conversions (IAEA, 2003):

$$1\,\%\,K = 1.505\ \mu R/h,$$
$$1\ ppm\ eU = 0.653\ \mu R/h,$$
$$1\ ppm\ eTh = 0.287\ \mu R/h.$$

5.5.9. Data Levelling and Smoothing

A visual inspection of the uranium ground concentration and total count grids revealed more or less strong along-line anomalies for some of the flights. The reason for these anomalies is most probably strongly varying atmospheric radon abundance during the survey. In order to eliminate the radon influence, an empirical, manual correction was applied to the uranium and total count data by subtracting different constant values for individual flights (**Table 23**). The correction was applied prior to the vegetation correction and the determination of exposure rates.

Table 23: *Values subtracted for radon correction*

Flight No.	U [ppm]	TC [cps]
13705	0.8	20
13706	0.5	10
13707	1.0	30
13708	1.0	50
13709	1.5	50

Remaining, mostly small level errors are eliminated in a subsequent micro-levelling process based on gridded line data in which level errors are identified using two-dimensional Butterworth high-pass (cut-off value: 600 m, degree: 8) and directional cosine FFT (azimuth: 148°, degree: 1) filters. Result of the filtering process is an error grid which is sampled along the flight lines. The sampled error values are heavily smoothed using a B-Spline filter (smoothness: 0.65, tension: 0.5) and then subtracted from the original data. Gridding of the levelled data yields grids that are virtually free of level errors. Finally, the tie-line data are fit to the levelled line-data grid. This is done by calculating the difference (error) between the values of the levelled line-data grid and the tie-line data, spline smoothing the error and subtracting it from the tie-line data.

Grids of the finally levelled data are slightly smoothed using a two-dimensional median filter of radius 1 (for potassium, thorium and total count) or 2 (for uranium) grid cells. The filtered grids are sampled along the flight path and the sampled data are used as input for vegetation attenuation correction and exposure rate calculations (see **Section 5.5.8**).

5.5.10. Presentation of the Results

The results of the gamma-ray survey are presented as maps of the equivalent concentrations of the radioelements potassium, uranium, and thorium, total count, and the ground level exposure rate. The maps produced to display the radiometric data are listed in **Section 6.3**. All data points used for map production are drawn as small black dots (flight lines). White dots mark areas of interpolated data.

6. Cartographic Work

6.1. Topographic Map

Topographic maps were produced for both map sheets (SW and NE) as the base maps for all thematic maps displaying the airborne geophysical results. A scale of 1:25,000 was chosen for the survey area. An UTM coordinate grid, based on the WGS 84 ellipsoid, is included on the topographic maps. **Table 24** contains the corner coordinates of the map sheet.

Table 24: *Coordinates of the corners of the 1:25,000 Friesland topographic map sheets*

Map corners	Geographic coordinates (WGS 84)		UTM WGS 84 coordinates (Zone 31N)	
	Easting	Northing	Easting	Northing
Sheet SW				
SW	5°23'38"	53°10'17"	660000	5894000
NW	5°23'59"	53°16'45"	660000	5906000
NE	5°41'58"	53°16'22"	680000	5906000
SE	5°41'34"	53°09'54"	680000	5894000
Sheet NE				
SW	5°32'49"	53°13'52"	670000	5901000
NW	5°33'12"	53°20'20"	670000	5913000
NE	5°51'12"	53°19'55"	690000	5913000
SE	5°50'47"	53°13'27"	690000	5901000

The map is based on the »Topografische Kaart van Nederland 1:25,000«, © Topografische Dienst, Emmen. The following map sheets were used:

5F Sint Annaparochie, 5G Franeker, 5H Dronrijp, 6A Ferwerd / Ferwert, 6C Leeuwarden.

The map has a digitally constructed border and tick marks indicating coordinates in the WGS 84 coordinate system. The grey-shading of the topography of the thematic map has a screen density of 50% of the original digital topographic map.

6.2. Map Production with GEOSOFT and GIS Software

The geophysical grids for the thematic maps were produced using the software package GEOSOFT OASIS montaj 7.2. **Table 25** shows the grid parameters used for the Friesland survey.

The final maps including geophysical, topographical and legend information are prepared using the program ESRI ArcGIS 9.3.1. A special plug-in provided by GEOSOFT for ArcGIS (available on DVD or http://www.geosoft.com/resources/releasenotes/plugins/arcGISplugin.asp) is necessary to import and display the GEOSOFT grids as a layer in ArcMap. Adobe Acrobat 9.3 is used for preparing the PDF documents.

Table 25: *Grid parameters*

Parameter	Value
Gridding method	Minimum curvature
Grid size [m]	50
Search radius [m]	50
Internal tension (0-1)	0
Cell extend beyond data	4
Log option	log ρ (else linear)

6.3. Thematic Maps

Coloured geophysical thematic maps (**Table 26**, **Appendix IV**) were produced at a scale of 1:25,000 for each parameter of interest.

HEM: Apparent resistivities and centroid depths
at 387 Hz, 1,821 Hz, 5,405 Hz, 8,388 Hz, 41,460 Hz, and 133,300 Hz;
Resistivities at 2, 4, 6, 8, 10, 15 ,20 and 25 m below sea level (bsl);

HMG: Anomalies of the total magnetic field;

HRD: Equivalent concentrations of the radioelements potassium, uranium, and thorium,
total count rate and ground level exposure rate.

The digital topographic map was used as base map. The surveyed flight lines are plotted in black/white containing information about the quality of the data. In addition, flight-line and elevations maps were produced.

The flight-line maps show the position of the surveyed profiles on the topographic maps. The corresponding line number is shown at the end of a profile at which the flight for that profile commenced. Positions of selected time marks (records), e. g., every 100th, are marked with an “×”. Every tenth plotted time mark is labelled with its number. The flight-line maps permit fast and easy correlation of data from profiles and vertical sections and their position in the survey area.

Digital elevation models (DEM) are derived from the corrected and levelled difference of bird elevation laser altitude. The elevation map also contains the topographic base map and the flight lines.

7. Archiving

All data sets and plots are stored on DVD and archived at BGR section B 2.1 – Geophysical Exploration – Resources and Near Surface Processes. The data formats of processed data are described in **Appendix II**. A technical report, the vertical sections, and the thematic maps (as PDF files) are stored together with the final data (ASCII-coded in GEOSOFT-XYZ format) on a DVD (**Table 25**). A copy of this DVD is attached to this report. The content is listed in **Appendix III**. **Appendix IV** and **Appendix V** contain copies of all maps and vertical resistivity sections, respectively, reduced to smaller scales fitting the A4 format of this report.

Table 26: *Content of the DVD*

Directory		Description of content
\Adobe Acrobat		Adobe® Acrobat Reader in diverse versions for popular system software
\Report		Technical report of the project in PDF format
\Data…	\HEM	ASCII file with all raw data (HEM137_RAW.xyz) ASCII file with all processed data (HEM137_DAT.xyz) ASCII file with all derived parameters (HEM137_APP.xyz) ASCII file with results of the 1-D inversion (HEM137_INV.xyz)
	\HMG	ASCII file with data of the total magnetic field, IGRF, base station data, diurnal variations etc. (HMG137.xyz)
	\HRD	ASCII file with data of the equivalent concentrations of potassium, uranium and thorium and the total count rate (HRD137.xyz)
\Maps…	\HEM	Apparent resistivity maps and centroid depth maps at a scale of 1:25,000 for the frequencies 387 Hz, 1,821 Hz, 5,405 Hz, 8,388 Hz, 41,460 Hz, 133,300 Hz in PDF format Resistivity maps at a scale of 1:25,000 at 2, 4, 6, 8, 10, 15, 20 and 25 m below sea level based on five-layer inversion results in PDF format
	\HMG	Magnetic anomalies maps at a scale of 1:25,000 in PDF format
	\HRD	Maps of the equivalent concentrations of the radioelements potassium, uranium, and thorium, the total count rate and the ground level exposure rate at a scale of 1:25,000 in PDF format
	\Flight lines	Flight-line maps with topography at a scale of 1:25,000 in PDF format
	\DEM	Digital elevation models at a scale of 1:25,000 in PDF format
	\ArcGIS	Map projects for ArcGIS 9.3.1 (*mxd) incl. legends (*bmp), Raster data TK 50 (GRID) and Geosoft-Plugin for ArcGIS
\Vertical sections		Vertical resistivity section based on five-layer inversion results for each profile of the survey area at a horizontal scale of 1:25,000 and at a vertical scale of 1:1,000 in PDF format

8. References

Anderson, W.L., 1989. A hybrid fast Hankel transform algorithm for electromagnetic modelling. Geophysics 54, 263–266.

Grasty, R.L., Holman, P.B. & Blanchard, Y.B., 1991. Transportable calibration pads for ground and airborne gamma-ray spectrometers. Geological survey of Canada, Paper 90-23, 25p.

Hovgaard, J., & Grasty, R.L., 1997. Reducing statistical noise in airborne gamma ray data through spectral component analysis. In "Proceedings of Exploration 97: Fourth Decennial Conference on Mineral Exploration" edited by A.G. Gubins, 753–764.

IAEA, 2003. Guidelines for radioelement mapping using gamma ray spectrometry data. International Atomic Energy Agency. IAEA-TECDOC-1363AEA, Vienna.

Mathis, G.L., 1987. Smoothing spectral gamma logs: A simple but effective technique. Geophysics, 52, 363–367.

IAGA, 1992. International Geomagnetic Reference Field, 1991 Revision. International Association of Geomagnetism and Aeronomy (IAGA) Division V, Working Group 8: Analysis of the main field and secular variation. Geophys. J. Int., 108, 945–946.

IAGA, 2005. International Geomagnetic Reference Field, 2005, 10th generation. International Association of Geomagnetism and Aeronomy, Division V, Working Group V-MOD. http://www.ngdc.noaa.gov/IAGA/vmod/igrf.html.

Johansen, H.K. and Sørensen, K., 1979. The fast Hankel transform. Geophysical Prospecting 27, 876–901.

Naudy, H. & Dreyer, H., 1968. Non-Linear Filtering Applied to Aeromagnetic Profiles. Geophysical Prospecting, 16, 171–178.

Sengpiel, K.-P. & Siemon, B., 2000. Advanced inversion methods for airborne electromagnetic exploration. Geophysics, 65, 1983–1992.

Siemon, B., 2001. Improved and new resistivity-depth profiles for helicopter electromagnetic data. J. Appl. Geophys., 46, 65–76.

Siemon, B., 2006. Electromagnetic methods – frequency domain: Airborne techniques. In: Kirsch, R. (ed.), Groundwater Geophysics – A Tool for Hydrogeology, Springer-Verlag, Berlin, Heidelberg, 155-170.

Siemon, B., 2009. Levelling of frequency-domain helicopter-borne electromagnetic data. Journal of Applied Geophysics, 67, 206–218.

Ward, S.H. & Hohmann, G.W., 1988. Electromagnetic theory for geophysical applications. In Nabighian M.N. (Eds.) Electromagnetic methods in applied geophysics Vol. 1, Theory. Society of Exploration Geophysics, IG no 3, Tulsa, 130–310.

Weidelt, P., 1991, Introduction into electromagnetic sounding. Lecture manuscript. Technical University of Braunschweig, Germany.

BUNDESANSTALT FÜR GEOWISSENSCHAFTEN UND ROHSTOFFE

BGR, HANOVER

(Dr. M. Kosinowski)	(Dr. U. Meyer)	(Dr. B. Siemon)
Head of Department „Groundwater and Soil Science“	Head of Sub-Department „Geophysical Exploration – Resources and Near Surface Processes“	Head of Unit „Airborne Geophysics“

Appendix I

Survey Area 137 – Friesland

Airport:	Leeuwarden, Elevation: 0 ft / 0 m			
Survey parameters:				
Line separation:	Lines:	250 m	Tie lines:	2000 m
Line direction:	Lines:	58°	Tie lines:	148°
Line kilometre:	Lines:	553 km	Tie lines:	63 km
Size of area:	162 km²			
Coordinate system:	WGS 84		UTM Zone 31N	
Location of base station:	X: 684150 (5°45'32"E		Y: 5901425 53°13'49"N)	

Table A-1: *Flight table*

Flight	Date	Time (UTC) Start – End	Lines	Remarks
13701	18.08.09	8:06 – 8:48	36.1 E 33.3 W 30.1 E	**HELIDAS**: SYS14; BKS36a (bird 61) **EM**: EM4/6 Amplitude and phase shift on all Profiles, system break down on line 30.1 **Magnetometer**: ok **Spectrometer**: ok **Video**: **Weather**: sunny, 20°C, no wind

13702	18.08.09	8:51 – 9:35	27.1 W 27.3 W 24.1 E	**HELIDAS**: SYS14; BKS36a (bird 61) **Continuation of flight 13701** **EM**: EM4 phase shift on all Profiles , EM6 Amplitude and phase shift on all Profiles, system break down on line 24.1 **Magnetometer**: ok **Spectrometer**: ok **Video**: **Weather**: sunny, 20°C, no wind
13703	18.08.09	12:06 – 13:20	2.1 E 3.1 W 4.1 E 5.1 W 6.1 E 7.1 W	**HELIDAS**: SYS14; BKS36a (bird 61) **EM**: System break down on line 7.1 flight split and renamed to 13710, 13711 and 13712 **Magnetometer**: ok **Spectrometer**: ok **Video**: **Weather**: sunny, 25°C, no wind
13704	18.08.09	13:24 – 14:25	10.1 E 11.1 W 12.1 E 13.1 W 14.1 E 15.1 W 16.1 E 17.1 W	**HELIDAS**: SYS14; BKS36a (bird 61) **Continuation of flight 13703** **EM**: ok **Magnetometer**: ok **Spectrometer**: ok **Video**: **Weather**: sunny, 20°C, no wind

13705	19.08.09	7:04 – 9:26	18.1 E 19.1 W 20.1 E 21.1 W 22.1 E 23.1 W 26.1 E 25.1 W 28.1 E 29.1 W 32.1 E 31.1 W 34.1 E 35.1 W 38.1 E	**HELIDAS**: SYS14; BKS36a (bird 61) **EM**: jumps in EM flight split and renamed to 13713, 13714 and 13715 **Magnetometer**: ok **Spectrometer**: ok **Video**: **Weather**: sunny, 17°C, no wind
13706	19.08.09	11:23 – 12:30	12.9 N 11.9 S 10.9 N 1.9 S 2.9 N 3.9 S	**HELIDAS**: SYS14; BKS36a (bird 61) **EM**: jumps in EM flight split and renamed to 13716 and 13717 **Magnetometer**: ok **Spectrometer**: ok **Video**: **Weather**: sunny, 25°C, no wind
13707	19.08.09	12:32 – 13:48	4.9 N 5.9 S 9.1 W 10.1 E 11.1 W 8.1 E	**HELIDAS**: SYS14; BKS36a (bird 61) **Continuation of flight 13706** **EM**: jumps in EM flight split and renamed to 13718 and 13719 **Magnetometer**: ok **Spectrometer**: ok **Video**: **Weather**: sunny, 25°C, no wind

13708	20.08.09	07:02 – 09:25	13.3 W 12.3 E 14.3 E 15.3 W 16.3 E 17.3 W 18.3 E 19.3 W 20.3 E 21.3 W 22.3 E 23.3 W 24.3 E 25.3 W 26.3 E 27.4 W 28.3 E 29.3 W 30.3 E 31.3 W 32.3 E 33.4 W 34.3 E 35.3 W	**HELIDAS**: SYS14; BKS36a (bird 61) **EM**: ok **Magnetometer**: ok **Spectrometer**: ok **Video**: **Weather**: sunny, 21°C, windy
13709	20.08.09	10:47 – 12:19	41.1 W 42.1 E 39.1 W 40.1 E 37.1 W	**HELIDAS**: SYS14; BKS36a (bird 61) **EM**: jumps in EM flight split and renamed to 13720 and 13721 **Magnetometer**: ok **Spectrometer**: ok **Video**: **Weather**: sunny, 28°C, windy

Appendix II

Final Data Format Description

A) Electromagnetics

Description of the four ASCII-coded data files containing the final (levelled) data of a helicopter-borne electromagnetic (HEM) survey

General HEADER:

```
/BGR HEADER (SHORT VERSION):
/
/AREANAME
/FRIESLAND
/AREACODE
/137
/C_MERIDIAN, ZONE, REFERENCE SYSTEM
/  3  31  WGS84
/ELLIPSOID FOR LON AND LAT
/WGS84
/BIRD
/61
/NUMFREQ
/ 6
/FREQUENCY
/     387.00     1821.00     5405.00     8388.00   41460.00 133300.00
/COILGEOMETRY
/         1.00          1.00          4.00          1.00          1.00          1.00
/COILSEPERATION
/         7.94          7.93          9.06          7.93          7.91          7.92
/TOWCABLE
/ 40.00
/DUMMY
/   -999.99
/DECIMATIONVALUE
/ 1
/PRIVTEXT
(up to five lines of comment may be written here)
```

1) Raw data: HEM137_RAW.XYZ

Example:

```
/Unprocessed data
//Flight 13701
//Date 2009/08/18
Random  0
/     X          Y   LON_BIRD_RAW  LAT_BIRD_RAW  RECORD   UTC_TIME   ALTR  ALTL_FP  ZHG_BIRD_RAW  ZHG_HELI_RAW  ALTB      EM1I       EM1Q    ...     EM6I     EM6Q EM1_FREQ...EM6_FREQ  CPPL    CPSP
  680754   5900367   5.707564      53.221804       0     80609.0  1567.54  450.57      445.60         491.60     303.96  -146056.13  -92952.99...  -16230.49  1749.15   41420 ...    5399   0.0011  0.0038
  680751   5900366   5.707521      53.221800       1     80609.1  1569.75  450.57      445.41         491.41     303.65  -146056.05   -92953.17  ...-16230.97  1748.93   41421 ...    5399   0.0013  0.0068
  680748   5900366   5.707477      53.221796       2     80609.2  1567.92  449.95      445.22         491.22     303.65  -146056.00  -92953.19...-16231.75    1748.85   41423 ...    5399   0.0018  0.0063
```

In this data file all secondary field values are stored in the order of the following description:

Channel	Unit	Remarks
X	m	UTM easting in m (WGS 84, Zone 31N), these coordinates have a false easting of 500000 metres
Y	m	UTM northing in m (WGS 84, Zone 31N), these coordinates have no false northing
LON	°	geographic longitude, reference system WGS 84
LAT	°	geographic latitude, reference system WGS 84
RECORD		time mark increasing by 1 every 0.1 seconds
UTC_TIME	hhmmss.s	GPS time (UTC)
ALTR	ft	radar altimeter reading (helicopter)
ALTL_FP	m	laser altimeter reading (bird)
ZHG_BIRD_RAW	m	GPS elevation of the bird, reference system WGS 84
ZHG_HELI_RAW	m	GPS elevation of the helicopter, reference system WGS 84
ALTB	ft	barometric elevation of the helicopter
EM1I	ppm	raw value of the inphase component at the frequency f = 41,460 Hz
EM1Q	ppm	raw value of the quadrature component at the frequency f = 41,460 Hz
EM2I	ppm	raw value of the inphase component at the frequency f = 8,388 Hz
EM2Q	ppm	raw value of the quadrature component at the frequency f = 8,388Hz
EM3I	ppm	raw value of the inphase component at the frequency f = 387 Hz
EM3Q	ppm	raw value of the quadrature component at the frequency f = 387 Hz
EM4I	ppm	raw value of the inphase component at the frequency f = 133,300 Hz
EM4Q	ppm	raw value of the quadrature component at the frequency f = 133,300 Hz
EM5I	ppm	raw value of the inphase component at the frequency f = 1,821 Hz
EM5Q	ppm	raw value of the quadrature component at the frequency f = 8,388 Hz
EM6I	ppm	raw value of the inphase component at the frequency f = 5,405 Hz
EM6Q	ppm	raw value of the quadrature component at the frequency f = 5,405 Hz

EM1_FREQ	Hz	frequency of EM1 channels (nominally f = 41,460 Hz)
EM2_FREQ	Hz	frequency of EM2 channels (nominally f = 8,388 Hz)
EM3_FREQ	Hz	frequency of EM3 channels (nominally f = 387 Hz)
EM4_FREQ	Hz	frequency of EM4 channels (nominally f = 133,300 Hz)
EM5_FREQ	Hz	frequency of EM5 channels (nominally f = 1,821 Hz)
EM6_FREQ	Hz	frequency of EM6 channels (nominally f = 5,405 Hz)
CPPL		power-line detector
CPSP		sferics detector

Remarks:

Lines starting with "/"	comment,
Lines starting with "//"	flight number and date,
Lines starting with "Random"	original flights.

Original vertical coaxial data are indicated by -1.00 (instead of 4.00 for converted data):

/COILGEOMETRY

/ 1.00 1.00 -1.00 1.00 1.00 1.00

General Remarks for the next three data sets:

Lines starting with "/"	comment,
Lines starting with "//"	flight number and date,
Lines starting with "Line"	lines,
Lines starting with "Tie"	tie lines.

2) Data: HEM137_DAT.XYZ

Example:

```
/Processing by A. Ullmann (BGR) using Oasis montaj
/Levelled data
/    X          Y          LON          LAT      RECORD    UTC     TOPO  H_RADAR  H_LASER BIRD_NN  H_BARO  REAL_1  QUAD_1 ... REAL_6  QUAD_6
//Flight 13710
//Date 2009/08/18
Line  2.1
 671086   5907292   5.566630   53.287197   6820   121709.0  0.81    36.24     33.91    34.71    32.51    708.74   585.46  ... 2512.42   288.46
 671089   5907294   5.566678   53.287212   6821   121709.1  0.73    35.81     33.85    34.58    32.88    715.02   594.56  ... 2544.01   289.02
 671092   5907296   5.566726   53.287224   6822   121709.2  0.66    36.66     33.77    34.43    31.76    721.48   603.81  ... 2577.14   289.82
```

In this data file all necessary position parameters and secondary field values are stored in the order of the following description:

Channel	**Unit**	**Remarks**
X	m	UTM easting in m (WGS 84, Zone 31N), these coordinates have a false easting of 500000 metres
Y	m	UTM northing in m (WGS 84, Zone 31N), these coordinates have no false northing
LON	°	geographic longitude, reference system WGS 84
LAT	°	geographic latitude, reference system WGS 84
RECORD		time mark increasing by 1 every 0.1 seconds
UTC_TIME	hhmmss.s	GPS time (UTC)
TOPO	m	levelled topographic elevation (in metres above sea level), derived from the difference of bird elevation (BIRD_NN) and bird altitude (H_LASER)
H_RADAR	m	smoothed value of the radar altitude minus the effective cable length (≈40 m) from the helicopter to the bird, corresponds to the bird altitude
H_LASER	m	smoothed value of the laser altimeter, corresponds to the bird altitude
BIRD_NN	m	smoothed bird elevation (in metres above sea level), reference system: WGS84
H_BARO	m	processed value of the barometric sensor minus the effective cable length (≈40 m) from the helicopter to the bird
REAL_1	ppm	processed value of the inphase component at the frequency f = 387 Hz
QUAD_1	ppm	processed value of the quadrature component at the frequency f = 387 Hz
REAL_2	ppm	processed value of the inphase component at the frequency f = 1,821 Hz
QUAD_2	ppm	processed value of the quadrature component at the frequency f = 1,821 Hz
REAL_3	ppm	processed value of the inphase component at the frequency f = 5,405 Hz, converted to horizontal coplanar
QUAD_3	ppm	processed value of the quadrature component at the frequency f = 5,405 Hz, converted to horizontal coplanar
REAL_4	ppm	processed value of the inphase component at the frequency f = 8,388 Hz
QUAD_4	ppm	processed value of the quadrature component at the frequency f = 8,388 Hz
REAL_5	ppm	processed value of the inphase component at the frequency f = 41,460 Hz
QUAD_5	ppm	processed value of the quadrature component at the frequency f = 41,460 Hz
REAL_6	ppm	processed value of the inphase component at the frequency f = 133,300 Hz
QUAD_6	ppm	processed value of the quadrature component at the frequency f = 133,300 Hz

3) Half-space parameters: HEM137_APP.XYZ

Example:

```
/Processing by A. Ullmann (BGR) using Oasis montaj
/Levelled data
/    X          Y          LON          LAT      RECORD  UTC     TOPO  H_RADAR H_LASER BIRD_NN  H_BARO RHOA_1 KDA_1 ZST_1 ... RHOA_6 KDA_6 ZST_6
//Flight 13710
//Date 2009/08/18
Line  2.1
 671086  5907292  5.566630  53.287197  6820  121709.0  0.81  36.24  33.91  34.71  32.51  1.11  2.17  15.63 ...  4.62  0.95  2.43
 671089  5907294  5.566678  53.287212  6821  121709.1  0.73  35.81  33.85  34.58  32.88  1.11  2.00  15.49 ...  4.48  0.88  2.34
 671092  5907296  5.566726  53.287224  6822  121709.2  0.66  36.66  33.77  34.43  31.76  1.12  1.85  15.36 ...  4.36  0.81  2.25
```

In this data file all necessary position parameters and half-space parameters are stored in the order of the following description:

Channel	**Unit**	**Remarks**
X	m	UTM easting in m (WGS 84, Zone 32N), these coordinates have a false easting of 500000 metres
Y	m	UTM northing in m (WGS 84, Zone 32N), these coordinates have no false northing
LON	°	geographic longitude, reference system WGS 84
LAT	°	geographic latitude, reference system WGS 84
RECORD		time mark increasing by 1 every 0.1 seconds
UTC_TIME	hhmmss.s	GPS time (UTC)
TOPO	m	levelled topographic elevation (in metres above sea level), derived from the difference of bird elevation (BIRD_NN) and bird altitude (H_LASER)
H_RADAR	m	smoothed value of the radar altitude minus the effective cable length (≈40 m) from the helicopter to the bird, corresponds to the bird altitude
H_LASER	m	smoothed value of the laser altimeter, corresponds to the bird altitude
BIRD_NN	m	smoothed bird elevation (in metres above sea level), reference system: WGS84
H_BARO	m	filtered value of the barometric sensor minus the effective cable length (≈40 m) from the helicopter to the bird
RHOA_1	Ωm	apparent resistivity at the frequency f = 387 Hz
KDA_1	m	apparent depth at the frequency f = 387 Hz
ZST_1	m	centroid depth at the frequency f = 387 Hz
RHOA_2	Ωm	apparent resistivity at the frequency f = 1,821 Hz
KDA_2	m	apparent depth at the frequency f = 1,821 Hz
ZST_2	m	centroid depth at the frequency f = 1,821 Hz
RHOA_3	Ωm	apparent resistivity at the frequency f = 5,405 Hz
KDA_3	m	apparent depth at the frequency f = 5,405 Hz
ZST_3	m	centroid depth at the frequency f = 5,405 Hz
RHOA_4	Ωm	apparent resistivity at the frequency f = 8,388 Hz
KDA_4	m	apparent depth at the frequency f = 8,388 Hz
ZST_4	m	centroid depth at the frequency f = 8,388 Hz
RHOA_5	Ωm	apparent resistivity at the frequency f = 41,460 Hz
KDA_5	m	apparent depth at the frequency f = 41,460 Hz
ZST_5	m	centroid depth at the frequency f = 41,460 Hz
RHOA_6	Ωm	apparent resistivity at the frequency f = 133,300 Hz
KDA_6	m	apparent depth at the frequency f = 133,300 Hz
ZST_6	m	centroid depth at the frequency f = 133,300 Hz

4) Inversion models HEM137_INV.XYZ

Example

```
/Processing by A. Ullmann (BGR) using Oasis montaj
/Levelled data
/   X         Y          LON         LAT      RECORD   UTC     TOPO  H_RADAR  H_LASER  BIRD_NN  H_BARO  RHO_I_1  D_I_1    ...   RHO_I_4  D_I_4  RHO_I_5  QALL
//Flight 13710
//Date 2009/08/18
Line  2.1
 671086  5907292  5.566630  53.287197  6820  121709.0 0.38   36.24    34.34    34.71    32.51    6.37    3.07    ...    1.01    6.65    1.01    1.66
 671089  5907294  5.566678  53.287212  6821  121709.1 0.39   35.81    34.19    34.58    32.88    6.60    2.92    ...    1.03    6.68    1.02    1.80
 671092  5907296  5.566726  53.287224  6822  121709.2 0.59   36.66    33.84    34.43    31.76    7.75    3.02    ...    0.98    6.72    1.05    1.41
```

In this data file all necessary position parameters and inversion models are stored in the order of the following description:

Channel	**Unit**	**Remarks**
X	m	UTM easting in m (WGS 84, Zone 31N), these coordinates have a false easting of 500000 metres
Y	m	UTM northing in m (WGS 84, Zone 31N), these coordinates have no false northing
LON	°	geographic longitude, reference system WGS 84
LAT	°	geographic latitude, reference system WGS 84
RECORD		time mark increasing by 1 every 0.1 seconds
UTC_TIME	hhmmss.s	GPS time (UTC)
TOPO	m	topographic elevation of the model surface (in metres above sea level), derived from the difference of bird elevation (BIRD_NN) and calculated bird altitude (H_LASER)
H_RADAR	m	smoothed value of the radar altitude minus the effective cable length (≈40 m) from the helicopter to the bird, corresponds to the bird altitude
H_LASER	m	calculated laser altitude, corresponds to the bird altitude above the model surface
BIRD_NN	m	smoothed bird elevation (in metres above sea level), reference system: WGS84
H_BARO	m	filtered value of the barometric sensor minus the effective cable length (≈40 m) from the helicopter to the bird
RHO_I_1	Ωm	resistivity of the top layer of a five-layer inversion model
D_I_1	m	thickness of the top layer of a five-layer inversion model
RHO_I_2	Ωm	resistivity of the second layer of a five-layer inversion model
D_I_2	m	thickness of the second layer of a five-layer inversion model
RHO_I_3	Ωm	resistivity of the third layer of a five-layer inversion model
D_I_3	m	thickness of the third layer of a five-layer inversion model
RHO_I_4	Ωm	resistivity of the fourth layer of a five-layer inversion model
D_I_4	m	thickness of the fourth layer of a five-layer inversion model
RHO_I_5	Ωm	resistivity of the fifth layer of a five-layer inversion model
QALL	%	misfit of the inversion (L1 norm)

Remarks:

The header contains following additional lines:

```
/IFREQUENCY
/   1     1     0     1     1     1
/NUMLAYER
/   5
/MUELAYER
/   0
```

B) Magnetics

Description of the ASCII coded data file **HMG137.XYZ** containing the final (levelled) data of a helicopter-borne magnetic (HMG) survey

```
/BGR HEADER:
/
/AREANAME
/FRIESLAND
/AREACODE
/137
/C_MERIDIAN, ZONE and GEOID FOR X and Y
/ 3 31 WGS84
/ELLIPSOID FOR LON AND LAT
/WGS84
/DEVICE
/G-822A
/IGRF
/2005
/LON_BASE
/53.2317047
/LAT_BASE
/5.7555938
/ALT_BASE
/1
/TOWCABLE
/ 40.0
/DUMMY
/   -9999
/PRIVTEXT
/ Processing by M. Ibs-von Seht
```

Example:

```
/   X          Y          LON          LAT       RECORD   UTC_DATE    UTC_TIME   ALT_BIRD    H_RADAR_RAW    H_LASER_RAW   T_BASE_RAW    T_BASE_F   T_RAW    DELTA_T    DELTA_T_LEV
//Flight 13703
//Date 2009/08/18
Line  2.1
671086   5907292  5.566630  53.287197  6820    20090818    121709.0     31.0        251.9          33.9     49192.04    49191.70  49235.45    36.53      36.70
671089   5907294  5.566678  53.287211  6821    20090818    121709.1     30.8        252.2          33.9     49192.04    49191.70  49235.46    36.57      36.74
671092   5907296  5.566726  53.287224  6822    20090818    121709.2     30.6        252.2          33.7     49192.04    49191.70  49235.48    36.61      36.77
```

In this data file all necessary position parameters and magnetic data are stored in the order of the following description:

Channel	**Unit**	**Remarks**
X	m	UTM easting in m (WGS 84, Zone 31N), these coordinates have a false easting of 500000 metres
Y	m	UTM northing in m (WGS 84, Zone 31N), these coordinates have no false northing
LON	°	geographic longitude, reference system WGS 84
LAT	°	geographic latitude, reference system WGS 84
RECORD		time mark increasing by 1 every 0.1 seconds
UTC_DATE	yyyymmdd	date
UTC_TIME	hhmmss.s	GPS time (UTC)
ALT_BIRD	m	smoothed bird elevation (in metres above sea level), reference system: WGS84
H_RADAR	m	smoothed value of the radar altitude minus the effective cable length (≈40 m) from the helicopter to the bird, corresponds to the bird altitude
H_LASER	m	smoothed value of the laser altimeter, corresponds to the bird altitude
T_BASE_RAW	nT	raw data of the magnetic field at the base station
T_BASE_F	nT	processed data of the magnetic field at the base station
T_RAW	nT	raw data of the magnetic field at the bird
DELTA_T	nT	anomalies of the magnetic field
DELTA_T_LEV	nT	levelled anomalies of the magnetic field

Remarks:

Lines starting with "/"	comment,
Lines starting with "//"	flight number and date,
Lines starting with "Line"	lines,
Lines starting with "Tie"	tie lines.

C) Radiometry

Description of the ASCII coded data file **HRD137.XYZ** containing the final (levelled) data of a helicopter-borne radiometric (HRD) survey

/BGR HEADER:
/
/AREANAME
/FRIESLAND
/AREACODE
/137
/C_MERIDIAN, ZONE and GEOID FOR X AND Y
/ 3 31 WGS84
/ELLIPSOID FOR LON AND LAT
/WGS84
/DEVICE
/GR-820
/BACKGROUND (IAEA 2003, S.60) a(TC), b(TC), a(K), b(K), a(U), b(U), a(Th), b(Th), a(upU), b(upU)
/31.09, 0.7224, 5.51, 0.0405, 0.48, 0.0326, 0.33, 0.0412, 0.0, 0.0090
/STRIPPING (IAEA 2003, S.65) alpha, beta, gamma
/0.2485, 0.3852, 0.6599
/ATTENUATION (IAEA 2003, S.67) mue(TC), mue(K), mue(U), mue(Th)
/-0.006468, -0.007733, -0.008132, -0.005784
/SENSITIVITY (IAEA 2003, S.68) S(K), S(U), S(Th)
/28.42, 2.916, 1.962
/TOWCABLE
/ 40.00
/DUMMY
/-9999
/PRIVTEXT
/Processed by M. Ibs-von Seht
Example:
/ X Y LON LAT RECORD UTC_DATE UTC_TIME ALT_BIRD H_RADAR_RAW H_LASER_RAW HAG PRESSURE TEMP LIVE_T COSMIC_RAW TOT_RAW POT_RAW URA_RAW THO_RAW URAUP_RAW
Continuation of last line:
TOT POT URA THO TOT_LEV POT_LEV URA_LEV THO_LEV EXPO
//Flight 13703
//Date 2009/08/18
Line 2.1

X	Y	LON	LAT	RECORD	UTC_DATE	UTC_TIME	ALT_BIRD	H_RADAR_RAW	H_LASER_RAW	HAG	PRESSURE	TEMP	LIVE_T	COSMIC_RAW	TOT_RAW	POT_RAW	URA_RAW	THO_RAW	URAUP_RAW
671086	5907292	5.566630	53.287197	6820	20090818	121709.0	31.0	251.9	34.0	79.0	101.935	20.6	937	75	667	85	15	29	2
671117	5907309	5.567109	53.287336	6830	20090818	121710.0	29.1	245.2	31.6	77.2	101.979	20.6	937	64	654	68	8	15	0
671149	5907325	5.567596	53.287472	6840	20090818	121711.0	26.4	238.0	29.6	74.7	102.010	20.6	946	60	698	86	14	25	3

Continuation of last three lines:

TOT	POT	URA	THO	TOT_LEV	POT_LEV	URA_LEV	THO_LEV	EXPO
661.4	2.12	2.67	12.12	675.55	2.29	2.59	10.86	8.26
661.3	2.15	2.41	12.15	672.18	2.27	2.58	11.01	8.25
662.0	2.20	2.01	12.39	668.72	2.24	2.57	11.17	8.26

In this data file all necessary position parameters and radiometric data are stored in the order of the following description:

Channel	**Unit**	**Remarks**
X	m	UTM easting in m (WGS 84, Zone 32N), these coordinates have a false easting of 500000 metres
Y	m	UTM northing in m (WGS 84, Zone 32N), these coordinates have no false northing
LON	°	geographic longitude, reference system WGS 84
LAT	°	geographic latitude, reference system WGS 84
RECORD		time mark increasing by 1 every 0.1 seconds
UTC_DATE	yyyymmdd	date
UTC_TIME	hhmmss.s	GPS time (UTC)
ALT_BIRD	m	smoothed bird elevation (in metres above sea level), reference system: WGS84
H_RADAR_RAW	m	value of the radar altitude minus the effective cable length (≈40 m) from the helicopter to the bird, corresponds to the bird altitude
H_LASER_RAW	m	value of the laser altimeter, corresponds to the bird
HAG	m	altitude of helicopter above ground level
PRESSURE	kPa	air pressure
TEMP	°C	air temperature
LIVE_T	ms	live time
COSMIC	cps	cosmic radiation > 3 MeV
TOT_RAW	cps	measured total count rate
POT_RAW	cps	measured potassium count rate
URA_RAW	cps	measured uranium count rate
THO_RAW	cps	measured thorium count rate
URAUP	cps	measured uranium count rate in upward looking crystal
TOT	cps	total count
POT	%	potassium concentration on ground level
URA	ppm	equivalent uranium concentration ground level
THO	ppm	equivalent thorium concentration ground level
TOT_LEV	cps	levelled total count, corrected for the effect of vegetation
POT_LEV	%	levelled potassium concentration on ground level, corrected for the effect of vegetation
URA_LEV	ppm	levelled equivalent uranium concentration on ground level, corrected for the effect of vegetation
THO_LEV	ppm	levelled equivalent thorium concentration on ground level, corrected for the effect of vegetation
EXPO	µR/h	ground level exposure rate

Remarks:

Lines starting with "/"	comment,
Lines starting with "//"	flight number and date,
Lines starting with "Line"	lines,
Lines starting with "Tie"	tie lines.

Appendix III

DVD

\Acrobat Reader
Adobe - Adobe Reader herunterladen.URL
\Linux\
AdbeRdr9.3.4-1_i486linux_deu.bin
\Mac\
AdbeRdr930_de_DE_i386.pkg.zip
\Windows\
AdbeRdr934_de_DE.exe

\Data
\HEM\
Format_description_HEM137.txt
HEM137_APP.xyz
HEM137_DAT.xyz
HEM137_INV.xyz
HEM137_RAW.xyz

\HMG\
Format_description_HMG137.txt
HMG137.XYZ

\HRD\
Format_description_HRD137.txt
HRD137.XYZ

\Maps
\ArcGis\
137 Friesland NE apparent resistivity rhoa1.mxd
137 Friesland NE apparent resistivity rhoa2.mxd
137 Friesland NE apparent resistivity rhoa3.mxd
137 Friesland NE apparent resistivity rhoa4.mxd
137 Friesland NE apparent resistivity rhoa5.mxd
137 Friesland NE apparent resistivity rhoa6.mxd
137 Friesland NE centroid depth zst1.mxd
137 Friesland NE centroid depth zst2.mxd
137 Friesland NE centroid depth zst3.mxd
137 Friesland NE centroid depth zst4.mxd
137 Friesland NE centroid depth zst5.mxd
137 Friesland NE centroid depth zst6.mxd
137 Friesland NE DEM.mxd
137 Friesland NE Exposure Rate.mxd
137 Friesland NE flight lines.mxd
137 Friesland NE magnetic anomalies.mxd
137 Friesland NE Potassium.mxd
137 Friesland NE resistivity -002m.mxd
137 Friesland NE resistivity -004m.mxd
137 Friesland NE resistivity -006m.mxd
137 Friesland NE resistivity -008m.mxd
137 Friesland NE resistivity -010m.mxd
137 Friesland NE resistivity -015m.mxd
137 Friesland NE resistivity -020m.mxd
137 Friesland NE resistivity -025m.mxd
137 Friesland NE Thorium.mxd
137 Friesland NE Total Count.mxd
137 Friesland NE Uranium.mxd
137 Friesland Nordost WGS.mxd
137 Friesland Südwest WGS.mxd
137 Friesland SW apparent resistivity rhoa1.mxd
137 Friesland SW apparent resistivity rhoa2.mxd
137 Friesland SW apparent resistivity rhoa3.mxd
137 Friesland SW apparent resistivity rhoa4.mxd
137 Friesland SW apparent resistivity rhoa5.mxd
137 Friesland SW apparent resistivity rhoa6.mxd
137 Friesland SW centroid depth zst1.mxd
137 Friesland SW centroid depth zst2.mxd
137 Friesland SW centroid depth zst3.mxd
137 Friesland SW centroid depth zst4.mxd
137 Friesland SW centroid depth zst5.mxd
137 Friesland SW centroid depth zst6.mxd
137 Friesland SW DEM.mxd
137 Friesland SW Exposure Rate.mxd
137 Friesland SW flight lines.mxd
137 Friesland SW magnetic anomalies.mxd
137 Friesland SW Potassium.mxd
137 Friesland SW resistivity -002m.mxd
137 Friesland SW resistivity -004m.mxd
137 Friesland SW resistivity -006m.mxd
137 Friesland SW resistivity -008m.mxd
137 Friesland SW resistivity -010m.mxd
137 Friesland SW resistivity -015m.mxd
137 Friesland SW resistivity -020m.mxd
137 Friesland SW resistivity -025m.mxd
137 Friesland SW Thorium.mxd
137 Friesland SW Total Count.mxd
137 Friesland SW Uranium.mxd

\ArcGis\Legends\
Legends Friesland.zip

\ArcGis\Oasis\
137_HMG_NE.map
137_HMG_NE.map.xml
137_HMG_NE.mdf
137_HMG_SW.map
137_HMG_SW.map.xml
137_HMG_SW.mdf
137_HRD_NE.map
137_HRD_NE.map.xml
137_HRD_NE.mdf
137_HRD_SW.map
137_HRD_SW.map.xml
137_HRD_SW.mdf
EXPO_NE.grd
EXPO_NE.grd.gi
EXPO_NE.grd.xml
EXPO_SW.grd
EXPO_SW.grd.gi
EXPO_SW.grd.xml
FWR_PLOT_137_1025.ps
FWR_PLOT_137_2025.ps
MAG_LEV_NE.grd
MAG_LEV_NE.grd.gi
MAG_LEV_NE.grd.xml
MAG_LEV_SW.grd
MAG_LEV_SW.grd.gi
MAG_LEV_SW.grd.xml
POT_BIO_NE.grd
POT_BIO_NE.grd.gi
POT_BIO_NE.grd.xml
POT_BIO_SW.grd
POT_BIO_SW.grd.gi
POT_BIO_SW.grd.xml
rho_002mbsl_ne.GRD
rho_002mbsl_ne.GRD.gi
rho_002mbsl_ne.GRD.xml
rho_002mbsl_NE.map
rho_002mbsl_NE.map.xml
rho_002mbsl_sw.GRD

rho_002mbsl_sw.GRD.gi
rho_002mbsl_sw.GRD.xml
rho_002mbsl_SW.map
rho_002mbsl_SW.map.xml
rho_004mbsl_ne.GRD
rho_004mbsl_ne.GRD.gi
rho_004mbsl_ne.GRD.xml
rho_004mbsl_NE.map
rho_004mbsl_NE.map.xml
rho_004mbsl_sw.GRD
rho_004mbsl_sw.GRD.gi
rho_004mbsl_sw.GRD.xml
rho_004mbsl_SW.map
rho_004mbsl_SW.map.xml
rho_006mbsl_ne.GRD
rho_006mbsl_ne.GRD.gi
rho_006mbsl_ne.GRD.xml
rho_006mbsl_NE.map
rho_006mbsl_NE.map.xml
rho_006mbsl_sw.GRD
rho_006mbsl_sw.GRD.gi
rho_006mbsl_sw.GRD.xml
rho_006mbsl_SW.map
rho_006mbsl_SW.map.xml
rho_008mbsl_ne.GRD
rho_008mbsl_ne.GRD.gi
rho_008mbsl_ne.GRD.xml
rho_008mbsl_NE.map
rho_008mbsl_NE.map.xml
rho_008mbsl_sw.GRD
rho_008mbsl_sw.GRD.gi
rho_008mbsl_sw.GRD.xml
rho_008mbsl_SW.map
rho_008mbsl_SW.map.xml
rho_010mbsl_ne.GRD
rho_010mbsl_ne.GRD.gi
rho_010mbsl_ne.GRD.xml
rho_010mbsl_NE.map
rho_010mbsl_NE.map.xml
rho_010mbsl_sw.GRD
rho_010mbsl_sw.GRD.gi
rho_010mbsl_sw.GRD.xml
rho_010mbsl_SW.map
rho_010mbsl_SW.map.xml
rho_015mbsl_ne.GRD
rho_015mbsl_ne.GRD.gi
rho_015mbsl_ne.GRD.xml
rho_015mbsl_NE.map
rho_015mbsl_NE.map.xml
rho_015mbsl_sw.GRD
rho_015mbsl_sw.GRD.gi
rho_015mbsl_sw.GRD.xml
rho_015mbsl_SW.map
rho_015mbsl_SW.map.xml
rho_020mbsl_ne.GRD
rho_020mbsl_ne.GRD.gi
rho_020mbsl_ne.GRD.xml
rho_020mbsl_NE.map
rho_020mbsl_NE.map.xml
rho_020mbsl_sw.GRD
rho_020mbsl_sw.GRD.gi
rho_020mbsl_sw.GRD.xml
rho_020mbsl_SW.map
rho_020mbsl_SW.map.xml
rho_025mbsl_ne.GRD
rho_025mbsl_ne.GRD.gi
rho_025mbsl_ne.GRD.xml
rho_025mbsl_NE.map
rho_025mbsl_NE.map.xml
rho_025mbsl_sw.GRD
rho_025mbsl_sw.GRD.gi
rho_025mbsl_sw.GRD.xml
rho_025mbsl_SW.map
rho_025mbsl_SW.map.xml
rhoa1_lev_iq_ne.GRD
rhoa1_lev_iq_ne.GRD.gi
rhoa1_lev_iq_ne.GRD.xml
rhoa1_lev_iq_sw.GRD
rhoa1_lev_iq_sw.GRD.gi
rhoa1_lev_iq_sw.GRD.xml
rhoa1_NE.map
rhoa1_NE.map.xml
rhoa1_SW.map
rhoa2_lev_iq_ne.GRD
rhoa2_lev_iq_ne.GRD.gi
rhoa2_lev_iq_ne.GRD.xml
rhoa2_lev_iq_sw.GRD
rhoa2_lev_iq_sw.GRD.gi
rhoa2_lev_iq_sw.GRD.xml
rhoa2_NE.map
rhoa2_NE.map.xml
rhoa2_SW.map
rhoa3_lev_iq_ne.GRD
rhoa3_lev_iq_ne.GRD.gi
rhoa3_lev_iq_ne.GRD.xml
rhoa3_lev_iq_sw.GRD
rhoa3_lev_iq_sw.GRD.gi
rhoa3_lev_iq_sw.GRD.xml
rhoa3_NE.map
rhoa3_NE.map.xml
rhoa3_SW.map
rhoa3_SW.map.xml
rhoa4_lev_iq_ne.GRD
rhoa4_lev_iq_ne.GRD.gi
rhoa4_lev_iq_ne.GRD.xml
rhoa4_lev_iq_sw.GRD
rhoa4_lev_iq_sw.GRD.gi
rhoa4_lev_iq_sw.GRD.xml
rhoa4_NE.map
rhoa4_NE.map.xml
rhoa4_SW.map
rhoa4_SW.map.xml
rhoa5_lev_iq_ne.GRD
rhoa5_lev_iq_ne.GRD.gi
rhoa5_lev_iq_ne.GRD.xml
rhoa5_lev_iq_sw.GRD
rhoa5_lev_iq_sw.GRD.gi
rhoa5_lev_iq_sw.GRD.xml
rhoa5_NE.map
rhoa5_NE.map.xml
rhoa5_SW.map
rhoa5_SW.map.xml
rhoa6_lev_iq_ne.GRD
rhoa6_lev_iq_ne.GRD.gi
rhoa6_lev_iq_ne.GRD.xml
rhoa6_lev_iq_sw.GRD
rhoa6_lev_iq_sw.GRD.gi
rhoa6_lev_iq_sw.GRD.xml
rhoa6_NE.map
rhoa6_NE.map.xml
rhoa6_SW.map
rhoa6_SW.map.xml
THO_BIO_NE.grd
THO_BIO_NE.grd.gi
THO_BIO_NE.grd.xml
THO_BIO_SW.grd
THO_BIO_SW.grd.gi
THO_BIO_SW.grd.xml
topo_lev_ne.GRD
topo_lev_ne.GRD.gi

topo_lev_ne.GRD.xml
topo_lev_sw.GRD
topo_lev_sw.GRD.gi
topo_lev_sw.GRD.xml
TOT_BIO_NE.grd
TOT_BIO_NE.grd.gi
TOT_BIO_NE.grd.xml
TOT_BIO_SW.grd
TOT_BIO_SW.grd.gi
TOT_BIO_SW.grd.xml
URA_BIO_NE.grd
URA_BIO_NE.grd.gi
URA_BIO_NE.grd.xml
URA_BIO_SW.grd
URA_BIO_SW.grd.gi
URA_BIO_SW.grd.xml
zst1_lev_iq_ne.GRD
zst1_lev_iq_ne.GRD.gi
zst1_lev_iq_ne.GRD.xml
zst1_lev_iq_sw.GRD
zst1_lev_iq_sw.GRD.gi
zst1_lev_iq_sw.GRD.xml
zst1_NE.map
zst1_NE.map.xml
zst1_SW.map
zst1_SW.map.xml
zst2_lev_iq_ne.GRD
zst2_lev_iq_ne.GRD.gi
zst2_lev_iq_ne.GRD.xml
zst2_lev_iq_sw.GRD
zst2_lev_iq_sw.GRD.gi
zst2_lev_iq_sw.GRD.xml
zst2_NE.map
zst2_NE.map.xml
zst2_SW.map
zst2_SW.map.xml
zst3_lev_iq_ne.GRD
zst3_lev_iq_ne.GRD.gi
zst3_lev_iq_ne.GRD.xml
zst3_lev_iq_sw.GRD
zst3_lev_iq_sw.GRD.gi
zst3_lev_iq_sw.GRD.xml
zst3_NE.map
zst3_NE.map.xml
zst3_SW.map
zst3_SW.map.xml
zst4_lev_iq_ne.GRD
zst4_lev_iq_ne.GRD.gi
zst4_lev_iq_ne.GRD.xml
zst4_lev_iq_sw.GRD
zst4_lev_iq_sw.GRD.gi
zst4_lev_iq_sw.GRD.xml
zst4_NE.map
zst4_NE.map.xml
zst4_SW.map
zst4_SW.map.xml
zst5_lev_iq_ne.GRD
zst5_lev_iq_ne.GRD.gi
zst5_lev_iq_ne.GRD.xml
zst5_lev_iq_sw.GRD
zst5_lev_iq_sw.GRD.gi
zst5_lev_iq_sw.GRD.xml
zst5_NE.map
zst5_NE.map.xml
zst5_SW.map
zst5_SW.map.xml
zst6_lev_iq_ne.GRD
zst6_lev_iq_ne.GRD.gi
zst6_lev_iq_ne.GRD.xml
zst6_lev_iq_sw.GRD
zst6_lev_iq_sw.GRD.gi
zst6_lev_iq_sw.GRD.xml
zst6_NE.map
zst6_NE.map.xml
zst6_SW.map
zst6_SW.map.xml

\ArcGis\Topography\
Google-Friesland.aux
Google-Friesland.rrd
Google-Friesland.tfw
Google-Friesland.tfwx
Google-Friesland.tif
Google-Friesland.tif.aux.xml
Google-Friesland.tif.gi
Google-Friesland.tif.xml
Project_05a.img
Project_05a.img.vat.dbf
Project_05a.rrd
Project_05f.img
Project_05f.img.vat.dbf
Project_05f.rrd
Project_05g.img
Project_05g.img.vat.dbf
Project_05g.rrd
Project_05h.img
Project_05h.img.vat.dbf
Project_05h.rrd
Project_06a.img
Project_06a.img.vat.dbf
Project_06a.rrd
Project_06b.img
Project_06b.img.vat.dbf
Project_06b.rrd
Project_06c.img
Project_06c.img.vat.dbf
Project_06c.rrd
Project_11a.img
Project_11a.img.vat.dbf
Project_11a.rrd

\DEM\
137 Friesland NE DEM.pdf
137 Friesland SW DEM.pdf

\Flightlines\
137 Friesland NE flight lines.pdf
137 Friesland SW flight lines.pdf

\HEM\
137 Friesland NE apparent resistivity rhoa1.pdf
137 Friesland NE apparent resistivity rhoa2.pdf
137 Friesland NE apparent resistivity rhoa3.pdf
137 Friesland NE apparent resistivity rhoa4.pdf
137 Friesland NE apparent resistivity rhoa5.pdf
137 Friesland NE apparent resistivity rhoa6.pdf
137 Friesland NE centroid depth zst1.pdf
137 Friesland NE centroid depth zst2.pdf
137 Friesland NE centroid depth zst3.pdf
137 Friesland NE centroid depth zst4.pdf
137 Friesland NE centroid depth zst5.pdf
137 Friesland NE centroid depth zst6.pdf
137 Friesland NE resistivity -002m.pdf
137 Friesland NE resistivity -004m.pdf
137 Friesland NE resistivity -006m.pdf
137 Friesland NE resistivity -008m.pdf
137 Friesland NE resistivity -010m.pdf
137 Friesland NE resistivity -015m.pdf
137 Friesland NE resistivity -020m.pdf
137 Friesland NE resistivity -025m.pdf
137 Friesland SW apparent resistivity rhoa1.pdf
137 Friesland SW apparent resistivity rhoa2.pdf

137 Friesland SW apparent resistivity rhoa3.pdf
137 Friesland SW apparent resistivity rhoa4.pdf
137 Friesland SW apparent resistivity rhoa5.pdf
137 Friesland SW apparent resistivity rhoa6.pdf
137 Friesland SW centroid depth zst1.pdf
137 Friesland SW centroid depth zst2.pdf
137 Friesland SW centroid depth zst3.pdf
137 Friesland SW centroid depth zst4.pdf
137 Friesland SW centroid depth zst5.pdf
137 Friesland SW centroid depth zst6.pdf
137 Friesland SW resistivity -002m.pdf
137 Friesland SW resistivity -004m.pdf
137 Friesland SW resistivity -006m.pdf
137 Friesland SW resistivity -008m.pdf
137 Friesland SW resistivity -010m.pdf
137 Friesland SW resistivity -015m.pdf
137 Friesland SW resistivity -020m.pdf
137 Friesland SW resistivity -025m.pdf

\HMG\
137 Friesland NE magnetic anomalies.pdf
137 Friesland SW magnetic anomalies.pdf

\HRD\
137 Friesland NE Exposure Rate.pdf
137 Friesland NE Potassium.pdf
137 Friesland NE Thorium.pdf
137 Friesland NE Total Count.pdf
137 Friesland NE Uranium.pdf
137 Friesland SW Exposure Rate.pdf
137 Friesland SW Potassium.pdf
137 Friesland SW Thorium.pdf
137 Friesland SW Total Count.pdf
137 Friesland SW Uranium.pdf

\Report\
Technical Report CLIWAT 137 Friesland.pdf

\VRS\
UI_1370019.PDF
UI_1370021.PDF
UI_1370029.PDF
UI_1370031.PDF
UI_1370039.PDF
UI_1370041.PDF
UI_1370049.PDF
UI_1370051.PDF
UI_1370059.PDF
UI_1370061.PDF
UI_1370071.PDF
UI_1370083.PDF
UI_1370093.PDF
UI_1370101.PDF
UI_1370103.PDF
UI_1370109.PDF
UI_1370111.PDF
UI_1370113.PDF
UI_1370119.PDF
UI_1370121.PDF
UI_1370123.PDF
UI_1370129.PDF
UI_1370131.PDF
UI_1370133.PDF
UI_1370141.PDF
UI_1370143.PDF
UI_1370151.PDF
UI_1370153.PDF
UI_1370161.PDF
UI_1370163.PDF
UI_1370171.PDF
UI_1370173.PDF
UI_1370181.PDF
UI_1370183.PDF
UI_1370191.PDF
UI_1370193.PDF
UI_1370201.PDF
UI_1370203.PDF
UI_1370211.PDF
UI_1370213.PDF
UI_1370221.PDF
UI_1370223.PDF
UI_1370231.PDF
UI_1370233.PDF
UI_1370241.PDF
UI_1370243.PDF
UI_1370251.PDF
UI_1370253.PDF
UI_1370261.PDF
UI_1370263.PDF
UI_1370271.PDF
UI_1370274.PDF
UI_1370281.PDF
UI_1370283.PDF
UI_1370291.PDF
UI_1370293.PDF
UI_1370301.PDF
UI_1370303.PDF
UI_1370311.PDF
UI_1370313.PDF
UI_1370321.PDF
UI_1370323.PDF
UI_1370331.PDF
UI_1370334.PDF
UI_1370341.PDF
UI_1370343.PDF
UI_1370351.PDF
UI_1370353.PDF
UI_1370361.PDF
UI_1370371.PDF
UI_1370381.PDF
UI_1370391.PDF
UI_1370401.PDF
UI_1370411.PDF
UI_1370421.PDF

Appendix IV

Maps

(reduced to a scale of 1:125,000)

CLIWAT – Adaptive and sustainable water management and protection of society and nature in an extreme climate

AIRBORNE GEOPHYSICAL SURVEY FRIESLAND / THE NETHERLANDS

FLIGHT LINES

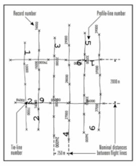

Tick marks indicated in the margin show **WGS84** coordinates, **Zone 31**. The grid in the map indicates the National Grid Rijksdriehoeksgrid. The topography was assembled from the following **base maps 1:25,000**:

5F Sint Annaparochie
5G Franeker
5H Dronrijp
6A Ferwerd / Ferwert
6C Leeuwarden

based on the Topografische Kaart van Nederland 1:25,000. © Topografische Dienst, Emmen

Scale 1:25 000 (4 cm ≙ 1 km)

0 0.5 1 1.5 2 2.5 3 km

Federal Institute for Geosciences and Natural Resources (BGR) Hanover, Federal Republic of Germany
TNO The Netherlands
Deltares The Netherlands
Wetterskip Fryslân The Netherlands
Provincje Fryslân The Netherlands
The project is co-financed by the European Union

Area: **Friesland (The Netherlands)**
Sheet: **NE**
Parameter: **Topography and flight lines**

Field operation and processing: **August 2009;** Malte Ibs-von Seht, Karl-Heinz Meinhardt, Jens Pielawa, Josef Scheiwein, Bernhard Siemon, Angelika Ullmann, Wolfgang Voß, Michael Schütt (Wiking Helikopter Service GmbH)

B 2.1 · Geophysical Exploration – Resources and Surface Processes · Aerogeophysics
Hanover 2010 · www.bgr.bund.de · heli@bgr.de

CLIWAT – Adaptive and sustainable water management and protection of society and nature in an extreme climate

AIRBORNE GEOPHYSICAL SURVEY FRIESLAND / THE NETHERLANDS

FLIGHT LINES

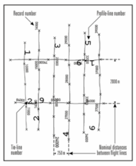

Tick marks indicated in the margin show **WGS84** coordinates, **Zone 31**. The grid in the map indicates the National Grid Rijksdriehoeksgrid. The topography was assembled from the following **base maps 1:25,000**:

5F Sint Annaparochie
5G Franeker
5H Dronrijp

based on the Topografische Kaart van Nederland 1:25,000. © Topografische Dienst, Emmen

Scale 1:25 000 (4 cm ≙ 1 km)

0 0.5 1 1.5 2 2.5 3 km

Federal Institute for Geosciences and Natural Resources (BGR) Hanover, Federal Republic of Germany
TNO The Netherlands
Deltares The Netherlands
Wetterskip Fryslân The Netherlands
Provincje Fryslân The Netherlands
The project is co-financed by the European Union

Area: **Friesland (The Netherlands)**
Sheet: **SW**
Parameter: **Topography and flight lines**

Field operation and processing: **August 2009;** Malte Ibs-von Seht, Karl-Heinz Meinhardt, Jens Pielawa, Josef Scheiwein, Bernhard Siemon, Angelika Ullmann, Wolfgang Voß, Michael Schütt (Wiking Helikopter Service GmbH)

B 2.1 · Geophysical Exploration – Resources and Surface Processes · Aerogeophysics
Hanover 2010 · www.bgr.bund.de · heli@bgr.de

Alle anderen Karten und Vertikal-
sektionen sind in dieser Web-Fassung
des Berichtes nicht enthalten.

All other maps and vertical
resistivity sections are not included
in this web edition of the report.